JCTC Journal of Chemical Theory and Computation

Article

pubs.acs.org/JCTC

Dioxygen Activation by a Non-Heme Iron(II) Complex: Theoretical Study toward Understanding Ferric−Superoxo Complexes

Hui Chen,*[,†,‡] Kyung-Bin Cho,[§] Wenzhen Lai,[‡,∥] Wonwoo Nam,*[,§] and Sason Shaik*[,‡]

[†]Beijing National Laboratory for Molecular Sciences (BNLMS), CAS Key Laboratory of Photochemistry, Institute of Chemistry, Chinese Academy of Sciences, Beijing, 100190, China

[‡]Institute of Chemistry and the Lise Meitner-Minerva Center for Computational Quantum Chemistry, The Hebrew University of Jerusalem, Givat Ram Campus, 91904 Jerusalem, Israel

[§]Department of Bioinspired Science, Department of Chemistry and Nano Science, Ewha Womans University, Seoul, 120-750, Korea

[∥]Department of Chemistry, Renmin University of China, Beijing, 100872, China

Supporting Information

ABSTRACT: We present a systematic study using density functional theory (DFT) and coupled cluster (CCSD(T)) computations with an aim of characterizing a non-heme ferric−superoxo complex $[(TMC)Fe(O_2)]^{2+}$ (TMC = 1,4,8,11-tetramethyl-1,4,8,11-tetraazacyclotetradecane) that was proposed to perform allylic C−H activation of cyclohexene (Lee, Y.-M. et al. *J. Am. Chem. Soc.* **2010**, *132*, 10668). As such, we investigated a series of iron−O_2 species without and with a sixth ligand bound to the iron ion in different O_2 coordination modes (end-on and side-on) and different spin states. Most of the iron−O_2 complexes were found to be iron(III)−superoxo species, Fe(III)(O_2^{-}), with high-spin (S = 5/2) or intermediate-spin (S = 3/2) ferric centers coupled ferromagnetically or antiferromagnetically to the superoxide anion radical. One iron(IV)−peroxo state, Fe(IV)(O_2^{2-}), was also examined. The preference for ferromagnetic or antiferromagnetic coupling modes between the superoxo and ferric radicals was found to depend on the FeOO angle, where a side-on tilt favors ferromagnetic coupling whereas the end-on tilt favors antiferromagnetic states. Experimental findings, e.g., the effects of solvent, spin state, and redox potential of non-heme Fe(II) complexes on O_2 activation, were corroborated in this work. Solvent effects were found to disfavor O_2 binding, relative to the unbound ferrous ion and O_2. The potential H-abstraction reactivity of the iron(III)−superoxo species was considered in light of the recently proposed exchange-enhanced reactivity principle (Shaik, S.; Chen, H.; Janardanan, D. *Nat. Chem.* **2011**, *3*, 19). It is concluded that localization and/or decoupling of an unpaired electron in the d-block of high-spin Fe(III) center in the S = 2 and 3 ferric−superoxo complexes during H abstractions enhances exchange stabilization and may be the root cause of the observed reactivity of $[(TMC)Fe(O_2)]^{2+}$.

I. INTRODUCTION

Mononuclear non-heme iron enzymes utilize O_2 in many biochemical oxidative transformations.[1] The corresponding synthetic analogues have provided a great deal of knowledge on the O_2 activation processes that lead to generation of non-heme high-valent iron(IV)−oxo complexes.[2−5] However, our understanding of the non-heme ferric−superoxo complexes (also known as iron−oxy in heme systems) is rather scant, as opposed to the well-studied oxy−heme complexes. It is well known by now that oxy−heme complexes prefer generally end-on geometries of the FeO_2 moiety and a singlet spin state, while the triplet and quintet states lie higher in energy.[6] In the non-heme analogs, however, it is still unclear whether the preferred Fe−O_2 coordination mode is side-on or end-on[7,8] and which spin states are preferred. The aim of this theoretical work is to draw a broad picture of the rich and complicated electronic structures of non-heme ferric−superoxo complexes by employing density functional theory (DFT) calculations calibrated by ab initio coupled cluster calculations with complete basis set (CBS) limit extrapolation, which to the best of our knowledge is the first such study.

Like heme iron−oxy species in O_2 activation,[9] the corresponding mononuclear non-heme complexes in enzymes and synthetic analogues have attracted considerable interest recently.[7,8,10−21] Non-heme ferric−superoxo complexes have been directly observed in naphthalene dioxygenase (NDO)[7] and homoprotocatechuate 2,3-dioxygenase (HPCD),[8] where it was found to be involved as an active oxidant. Significant progress has also been made over the past decade in providing synthetic ferric−superoxo complexes as intermediates during O_2 activation en route to the high-valent iron(IV)−oxo species.[22−27] For example, as shown in Scheme 1, several research groups have exploited O_2 activation reactivity of synthetic non-heme iron(II) complexes, such as Fe(II)(TMC) (TMC = 1,4,8,11-tetramethyl-1,4,8,11-tetraazacyclotetradecane), Fe(II)(TMC-py) (TMC-py = 1-(2′-pyridylmethyl)-4,8,11-trimethyl-1,4,8,11-tetraazacyclotetradecane), Fe(II)(TPA) (TPA = tris(2-pyridylmethyl)amine), Fe(II)(N4Py) (N4Py = *N*,*N*-bis(2-pyridylmethyl)-bis(2-pyridyl)-methylamine), Fe(II)(BPMEN) (BPMEN = *N*,*N*′-bis(2-pyridylmethyl)-1,2-diaminoethane), and Fe(II)(Bn-TPEN) (Bn-TPEN = *N*-benzyl-*N*,*N*′,*N*′-tris(2-pyridylmethyl)-1,2-diaminoethane).[24−27] Among these, the iron complexes with the TMC and its derivative ligands exhibited putative O_2 activation to yield the iron(IV)−oxo oxidant. It was first found by Nam and co-workers that

Received: January 9, 2012
Published: February 3, 2012

Scheme 1. Several Non-Heme Fe(II) Complexes Used for O_2 Activation Reactions in Experiments

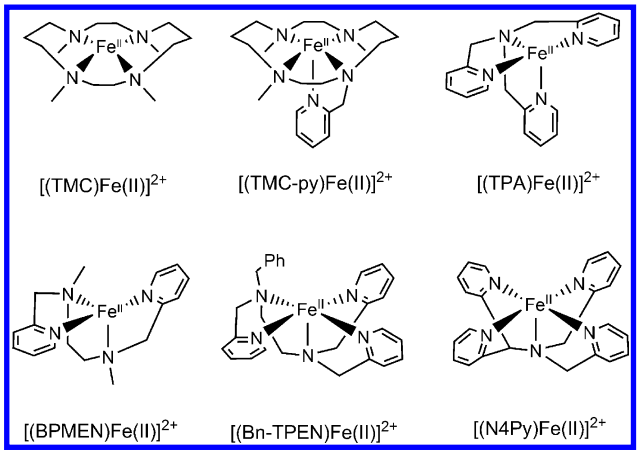

$[(TMC)Fe(II)]^{2+}$ can react with O_2 to generate $[(TMC)Fe(IV)(O)]^{2+}$ in mixed solvents of CH_3CN and ethanol without any additional electron and proton sources, although this O_2 activation process does not occur in pure CH_3CN solvent.[24] Other non-heme complexes, such as $[(N4Py)Fe(II)]^{2+}$, $[(TPA)Fe(II)]^{2+}$, and $[(BPMEN)Fe(II)]^{2+}$, do not react with O_2 under the same reaction conditions to afford the corresponding Fe(IV)(O) complexes. Subsequently, Que, Banse, and co-workers[27] and Nam, Fukuzumi, and co-workers[25] reported that adding electron and proton sources into the system could facilitate O_2 activation. For instance, adding BPh_4^- or BNAH (1-benzyl-1,4-dihydronicotinamide)[25,27] as an electron source and $HClO_4$ as a proton source in CH_3CN solvent induced the nonreactive $[(TMC)Fe(II)]^{2+}$ (and its derivatives like $[(TMC\text{-}py)Fe(II)]^{2+}$) to activate O_2 and generate the corresponding Fe(IV)(O) complexes. The nonreactive species like $[(N4Py)Fe(II)]^{2+}$ in mixed CH_3CN/alcohol solvent also turned reactive by adding an electron and proton source, albeit producing $[(N4Py)Fe(III)(OOH)]^{2+}$ rather than $[(N4Py)Fe(IV)(O)]^{2+}$. Most recently, Nam, Fukuzumi, and co-workers found that $[(TMC)Fe(II)]^{2+}$ in the presence of O_2 can generate $[(TMC)Fe(IV)(O)]^{2+}$ by performing allylic C−H bond activation of cyclic olefins.[26] Here the abstracted H atom turns out to be effectively equivalent to the electron and proton sources used before. A putative iron(III)−superoxo complex, $[(TMC)Fe(III)(O_2)]^{2+}$, was proposed as an active oxidant that, surprisingly, exhibits an H-abstraction reactivity which is even greater than that of the corresponding high-valent iron−oxo complex, $[(TMC)Fe(IV)(O)]^{2+}$, which does not react with the cyclic olefins used in the study.

Thus, it is clear that experiments have uncovered interesting chemistry of non-heme ferric−superoxo species, for which theoretical explorations are still scant. For example, experiments showed that the spin state of the non-heme Fe(II) system plays a crucial role in their O_2 activation reactivity.[24,25] However, the details of this spin state issue are not yet known, and this poses an appealing aspect for theoretical examination of non-heme ferric−superoxo complexes. In this work, we explore in detail various electronic structures of $[(TMC)Fe(O_2)]^{2+}$ species and its model complexes by employing DFT and ab initio CCSD(T) methods; the latter not only calibrates our DFT results but also represents the first example of high-level ab initio assessment of DFT computations for non-heme ferric−superoxo species, thus providing a guide for future theoretical exploration for non-heme ferric−superoxo systems.[28,29]

II. COMPUTATIONAL DETAILS

DFT Calculations. All DFT calculations for non-heme ferric−superoxo with TMC as a ligand were done using Gaussian 09.[30] The hybrid B3LYP functional[31] was used throughout this study with unrestricted formalism. Geometry optimizations were performed in a solvent employing an implicit solvation model, CPCM,[32] with acetonitrile solvent parameters. Frequency calculations were performed for all optimized stationary points to ensure that they are true minima. Free energies at 298.15 K were calculated based on vibrational analyses.

The basis set used in DFT calculation for geometry optimization is LACVP (B1),[33] which has been widely used for transition-metal-containing systems and has an effective potential that accounts for the scalar relativistic effects in iron. The UB3LYP/B1 energies are then corrected with a larger basis set, LACV3P+*,[33] hence, B2. The empirical dispersion correction of DFT (DFT-D3)[34] with short-range zero damping is also employed in our DFT calculations for the $[(TMC)Fe(O_2)]^{2+}$ model. As shown in Figure 1 below, we consider only

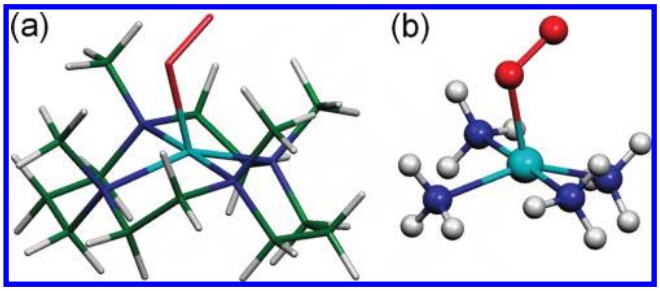

Figure 1. Truncation of the $[(TMC)Fe(O_2)]^{2+}$ system (a) to get the corresponding $[(NH_3)_4Fe(O_2)]^{2+}$ model (b).

the results for the complex wherein the O_2 ligand is on the same side as the four methyl groups of (TMC)Fe, because DFT calculations show that this is more stable than the complex where O_2 is coordinated in the opposite face of (TMC)Fe (see Table S2, Supporting Information). In addition, the most recent crystal structure of $[(TMC)Fe(O_2)]^+$ strongly suggests that this conformation, wherein O_2 and four methyl groups are on the same side of TMC ring, is most likely the preferred one.[19]

Ab Initio Calculations. Coupled cluster calculations in vacuum at the RCCSD(T) level were done with Molpro.[35] As in our previous work,[28a,29] the restricted open-shell KS orbitals from DFT(B3LYP) were used as reference for RCCSD(T) calculation. The scalar relativistic effect was included using the Douglas−Kroll−Hess (DKH) Hamiltonian[36] at second order in association with the Douglas−Kroll contraction of correlation-consistent basis sets. Due to the high computational expense of the RCCSD(T) calculation for our $[(TMC)Fe(O_2)]^{2+}$ system without molecular symmetry, we have to truncate the TMC ligand as shown in Figure 1b. Truncation results in model complexes $[(NH_3)_4Fe(O_2)]^{2+}$ from the various $[(TMC)Fe(O_2)]^{2+}$ structures obtained by DFT optimization. The positions of the non-hydrogen atoms were kept exactly the same as those in the $[(TMC)Fe(O_2)]^{2+}$ structures. The direction of the N−H bonds in $[(NH_3)_4Fe(O_2)]^{2+}$ was retained exactly the same as the C−C bonds in the $[(TMC)Fe(O_2)]^{2+}$ structures that were truncated. All N−H bond lengths were fixed at 1.0 Å, a distance which is very close to the N−H equilibrium bond length. The advantage of this truncation mode is the conservation of the immediate coordinate sphere environment of

dx.doi.org/10.1021/ct300015y | J. Chem. Theory Comput. 2012, 8, 915−926

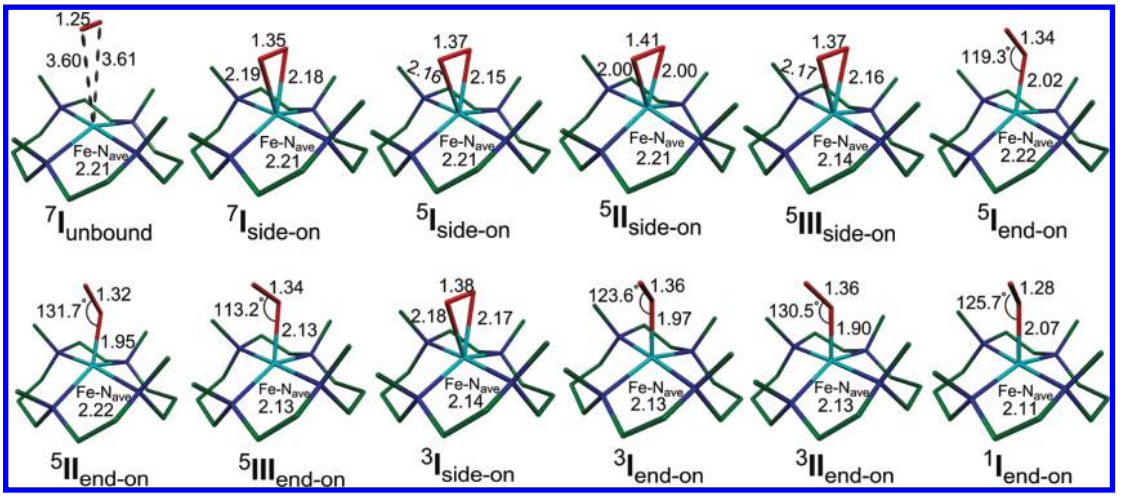

Figure 2. Optimized geometries of various non-heme $[(TMC)Fe(O_2)]^{2+}$ species.

Table 1. UB3LYP/CPCM/B2 Relative Energies (kcal/mol) for the Species of $[(TMC)Fe(O_2)]^{2+}$ Shown in Figure 2

state[a]	valence shell occupancy[b]		ΔE[c]	$\Delta(E+ZPE)$[d]	$\Delta(E+ZPE+D)$[e]	ΔG_{298}[f]
^{7}I$_{unbound}$	$^{\uparrow}d_{xy}\ ^{\uparrow}d_{xz}\ ^{2}d_{yz}\ ^{\uparrow}d_{z^2}\ ^{\uparrow}d_{x^2-y^2}\ ^{\uparrow}\pi^*_{\parallel}\ ^{\uparrow}\pi^*_{\perp}$	Fe(II)	0.0	0.0	0.0	0.0
^{7}I$_{side-on}$	$^{\uparrow}d_{xy}\ ^{\uparrow}d_{xz}\ ^{\uparrow}d_{yz}\ ^{\uparrow}d_{z^2}\ ^{\uparrow}d_{x^2-y^2}\ ^{2}\pi^*_{\parallel}\ ^{\uparrow}\pi^*_{\perp}$	Fe(III)	9.6	10.6	7.0	9.5
^{5}I$_{side-on}$	$^{\uparrow}d_{xy}\ ^{\uparrow}d_{xz}\ ^{\uparrow}d_{yz}\ ^{\uparrow}d_{z^2}\ ^{\uparrow}d_{x^2-y^2}\ ^{2}\pi^*_{\parallel}\ ^{\downarrow}\pi^*_{\perp}$	Fe(III)	14.3	15.2	11.6	14.3
^{5}II$_{side-on}$	$^{\uparrow}d_{xy}\ ^{\uparrow}d_{xz}\ ^{\uparrow}d_{yz}\ ^{\uparrow}d_{z^2}\ ^{\uparrow}d_{x^2-y^2}\ ^{\downarrow}\pi^*_{\parallel}\ ^{2}\pi^*_{\perp}$	Fe(IV)	21.8	22.6	18.3	20.9
^{5}III$_{side-on}$	$^{2}d_{xy}\ ^{\uparrow}d_{xz}\ ^{\uparrow}d_{yz}\ ^{\uparrow}d_{z^2}\ ^{0}d_{x^2-y^2}\ ^{2}\pi^*_{\parallel}\ ^{\uparrow}\pi^*_{\perp}$	Fe(III)	16.9	18.9	13.6	16.8
^{5}I$_{end-on}$	$^{\uparrow}d_{xy}\ ^{\uparrow}d_{xz}\ ^{\uparrow}d_{yz}\ ^{\uparrow}d_{z^2}\ ^{\uparrow}d_{x^2-y^2}\ ^{2}\pi^*_{\parallel}\ ^{\downarrow}\pi^*_{\perp}$	Fe(III)	13.6	14.2	12.1	14.0
^{5}II$_{end-on}$	$^{\uparrow}d_{xy}\ ^{\uparrow}d_{xz}\ ^{\uparrow}d_{yz}\ ^{\uparrow}d_{z^2}\ ^{\uparrow}d_{x^2-y^2}\ ^{\downarrow}\pi^*_{\parallel}\ ^{2}\pi^*_{\perp}$	Fe(III)	13.6	14.2	12.2	14.3
^{5}III$_{end-on}$	$^{2}d_{xy}\ ^{\uparrow}d_{xz}\ ^{\uparrow}d_{yz}\ ^{\uparrow}d_{z^2}\ ^{0}d_{x^2-y^2}\ ^{2}\pi^*_{\parallel}\ ^{\uparrow}\pi^*_{\perp}$	Fe(III)	18.5	21.0	16.7	19.9
^{3}I$_{side-on}$	$^{2}d_{xy}\ ^{\uparrow}d_{xz}\ ^{\uparrow}d_{yz}\ ^{\uparrow}d_{z^2}\ ^{0}d_{x^2-y^2}\ ^{2}\pi^*_{\parallel}\ ^{\downarrow}\pi^*_{\perp}$	Fe(III)	21.8	24.4	19.2	22.8
^{3}I$_{end-on}$	$^{2}d_{xy}\ ^{\uparrow}d_{xz}\ ^{\uparrow}d_{yz}\ ^{\uparrow}d_{z^2}\ ^{0}d_{x^2-y^2}\ ^{2}\pi^*_{\parallel}\ ^{\downarrow}\pi^*_{\perp}$	Fe(III)	19.3	21.1	16.3	19.1
^{3}II$_{end-on}$	$^{2}d_{xy}\ ^{\uparrow}d_{xz}\ ^{\uparrow}d_{yz}\ ^{\uparrow}d_{z^2}\ ^{0}d_{x^2-y^2}\ ^{\downarrow}\pi^*_{\parallel}\ ^{2}\pi^*_{\perp}$	Fe(III)	21.1	23.8	18.9	22.3
^{1}I$_{end-on}$	$^{2}d_{xy}\ ^{2}d_{xz}\ ^{\uparrow}d_{yz}\ ^{\uparrow}d_{z^2}\ ^{0}d_{x^2-y^2}\ ^{\downarrow}\pi^*_{\parallel}\ ^{\downarrow}\pi^*_{\perp}$	Fe(II)	17.3	19.5	14.9	18.7

[a]The left-hand superscript signifies the spin state of the species. [b]These representative Fe-O_2 valence shell occupancy are based on the UB3LYP spin density distribution. The interacting valence shells of Fe and O_2 orbitals are ordered from left to right: five iron 3d orbitals and two O−O π^* orbitals in ($\pi^*_{\parallel}$) or perpendicular ($\pi^*_{\perp}$) to the FeOO plane. *x* and *y* approximately parallel the Fe−N bonds: *y* parallels the slightly longer pair of trans Fe−N bonds, which is almost linear; *x* parallels the other pair of trans Fe−N bonds, which has an apparent nonlinear trans N−Fe−N structure (about 150°). [c]UB3LYP/CPCM/B2 electronic energy. [d]UB3LYP/CPCM/B2 electronic energy with zero-point energy (ZPE) correction. [e]UB3LYP/CPCM/B2 electronic energy with ZPE and DFT empirical dispersion corrections. [f]UB3LYP/CPCM/B2 electronic energy with DFT empirical dispersion corrections and thermal free energy corrections at 298 K.

iron when changing the TMC ligand to the four NH_3 ligands, thereby mimicking the TMC coordination as much as possible. Thus, the generated $[(NH_3)_4Fe(O_2)]^{2+}$ structure offers a reasonable model with which to assess the intrinsic spin state gap of the FeO_2 center without complication from factors like the strain energy of the macrocyclic ligand TMC, which is well treated by DFT in the full model, with inclusion of empirical dispersion correction.

To alleviate the potential basis set insufficiency problem in CCSD(T) calculations of relative energies, a two-point CBS limit extrapolation was employed based on Helgaker's inverse cubic scaling dependence of the correlation energy on the basis set.[37] Using uniform basis sets up to quadruple-ζ is prohibitively expensive for the $[(NH_3)_4Fe(O_2)]^{2+}$ model without any symmetry. To make the CBS calculation feasible, we partitioned the $[(NH_3)_4Fe(O_2)]^{2+}$ model into two parts (I and II) and used two basis sets. Part I is the central FeO_2; part II contains the four coordinating NH_3 ligands. In the CBS extrapolation, part I was described with cc-pVTZ-DK or cc-pVQZ-DK[38,39] while part II was described with cc-pVDZ-DK and then combined with part I using one of the above two basis sets (denoted as T/D and Q/D, for basis sets used in part I/part II). The CBS(∞/D) result was then obtained through T/D to Q/D extrapolation. To make sure that the basis set for part II is sufficient, we also used the larger basis set cc-pVTZ-DK[38,39] for part II and combined it with part I using the same basis set (denoted as T/T). From these T/T and T/D results, we obtained CBS(T/∞) values and estimated thereby the effect of augmented basis sets on part II. Subsequently, the CBS(∞/∞) estimate was derived by combining CBS(∞/D) and CBS(T/∞) calculations. The result shows that the CBS(T/∞) improvements over T/D result are usually very small, thus indicating that use of the larger basis set for the coordination sphere plays a minor role in the spin state gap calculation of the central ferric−superoxo unit, which is in line with our previous experience of non-heme iron−oxo species.[29]

Since we aim to get accurate reference data from the CCSD(T)/CBS calculations, we must also account for the iron semicore 3s3p correlation, which may affect the results. In addition, we used the cc-pwCVTZ-DK basis set on iron to treat the iron 3s3p correlation properly, which has a special augmentation for the semicore shell compared with the valence-only correlation

bases used above. This core−valence basis set for iron is combined with T/D basis sets for all other atoms to generate basis sets denoted as T_w/D for the CCSD(T) calculations. The 3s3p correction for the spin state gaps was calculated by the difference of two CCSD(T) single-point calculations with and without 3s3p electrons correlated using the same T_w/D basis set. This correction was added into the corresponding CCSD(T)/CBS(∞/∞) value from valence-only correlation as our final estimation of the energetics.

III. RESULTS AND DISCUSSIONS

The experiments utilizing (TMC)Fe(II) for O_2 activation did not allow for direct observation of the ferric−superoxo intermediate.[24−26] As such, the theoretical approach remains the only way of exploring this missing piece of non-heme chemistry. In our calculations, the reference energy for the various species is the optimized septet O_2·(TMC)Fe van der Waals cluster, composed of a triplet ground state O_2 coupled ferromagnetically with the high-spin (HS) quintet (TMC)Fe(II) complex. This cluster is denoted herein as $^7\mathbf{I}_{unbound}$ because O_2 and (TMC)Fe(II) are not chemically bonded in the cluster. All of the optimized structures for $[(TMC)Fe(O_2)]^{2+}$ in the solvent within 25 kcal/mol from $^7\mathbf{I}_{unbound}$ are depicted in Figure 2, while the calculated energetics and Fe-O_2 valence shell occupancies for $[(TMC)Fe(O_2)]^{2+}$ at the B3LYP/CPCM/B2 level are collected in Table 1. Since the calculated electronic energies shown in Table 1 are all quite close to the calculated free energies, unless specified otherwise, we shall discuss below only electronic energies.

Septet State (*S* = 3). As mentioned above, the septet O_2·(TMC)Fe van der Waals complex involves O_2 in a "side-on" orientation with a very long Fe−O distance of about 3.6 Å, as shown in Figure 2. The singly occupied molecular orbitals (SOMOs) of $^7\mathbf{I}_{unbound}$ are depicted in Figure 3 and clearly show

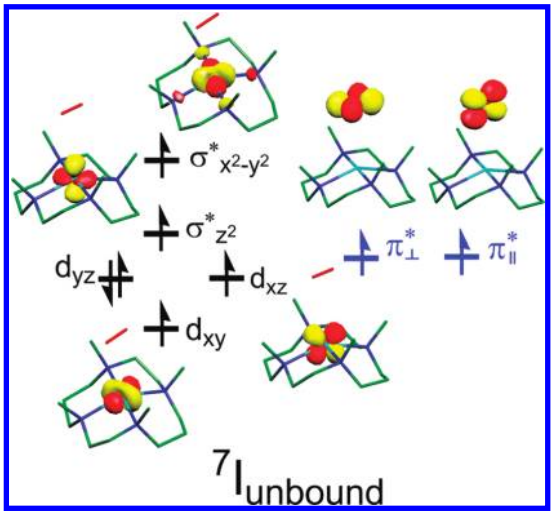

Figure 3. Electronic configuration of $^7\mathbf{I}_{unbound}$.

that O_2 has two unpaired electrons, while four others reside on the ferrous Fe(II) center, thus forming a HS Fe(II) (*S* = 2) combined ferromagnetically (F) with a triplet O_2 (*S* = 1). Due to the long O_2 to Fe(II) distance, there is only a tiny gap of 0.007 kcal/mol between $^7\mathbf{I}_{unbound}$ and the corresponding slightly higher antiferromagnetically (AF) coupled triplet O_2·(TMC)Fe complex (data not shown). The $^7\mathbf{I}_{unbound}$ species is our zero reference for all calculated relative energies.

Having $^7\mathbf{I}_{unbound}$ as a reference, we obtained a septet $^7\mathbf{I}_{side\text{-}on}$ complex in Figure 2, wherein O_2 is bound side-on and is an iron(III)−superoxo complex. The electronic structure of $^7\mathbf{I}_{side\text{-}on}$ is schematically shown in Figure 4. It is seen that O_2 here is a superoxide, having a singly occupied $\pi^*_\perp$, which is perpendicular to the Fe−OO plane, while the other doubly occupied π^* orbital ($\pi^*_\parallel$, in Fe−OO plane) forms a 3-e bond with the iron d_{xz} orbital. An alternative way to look at it is to consider the combinations of the d_{xz} orbital with $\pi^*_\parallel$ to form two new orbitals $d_{xz} \pm \pi^*_\parallel$, as shown in Figure 4. Thus, $^7\mathbf{I}_{side\text{-}on}$ is a hexaradicaloid

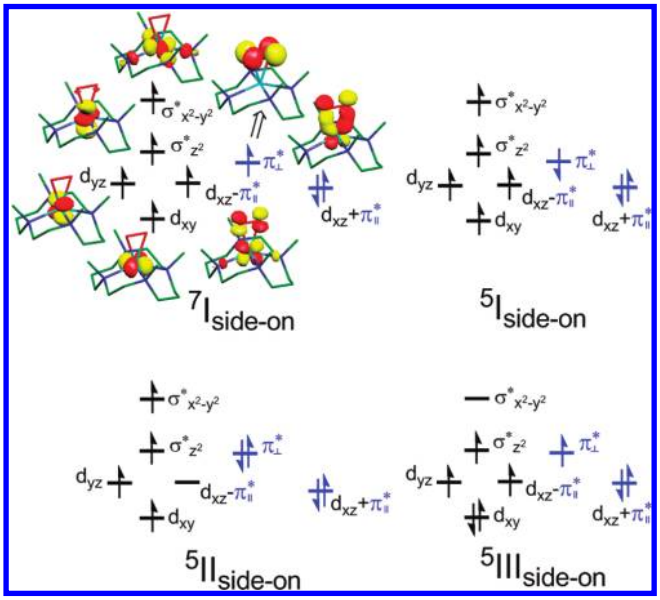

Figure 4. Electronic configurations of side-on septet and quintet states of $[(TMC)Fe(O_2)]^{2+}$.

state that involves F coupling of *S* = 5/2 Fe(III) with the *S* = 1/2 superoxo anion O_2^-. The DFT-calculated relative free energy of $^7\mathbf{I}_{side\text{-}on}$ is 9.5 kcal/mol, which is almost identical to the relative electronic energy of 9.6 kcal/mol at the B3LYP/CPCM/B2 level. In the gas phase, we also obtained a septet minimum giving a linear Fe−O−O angle and the same configuration as $^7\mathbf{I}_{unbound}$ (quintet Fe(II) F coupled with triplet O_2). However, during optimization of this linear structure in the solvent O_2 dissociates, which means that this complex will not be relevant in solution-phase processes. Therefore, it is unlikely that there exists a septet Fe−O_2 end-on structure in $[(TMC)Fe(O_2)]^{2+}$. This is consistent with a previous negative result of a computational search for an end-on septet FeO_2 structure in a non-heme enzyme.[13a] Despite these results, it should also be noted that a linear septet FeO_2 minimum was located in the $[(N4Py)Fe(O_2)]^{2+}$ system in the solvent.[3n]

Quintet State (*S* = 2). In total, we obtained six quintet state structures, three of which are side-on species while the other three are end-on ones. All six species are labeled as $^5(\mathbf{I/II/III})_{side\text{-}on/end\text{-}on}$ (see Figure 2), and except for one, all are iron(III)−superoxo complexes. States labeled with **I** and **II** have six unpaired electrons, and the state labeled with **III** has four unpaired electrons. We present below our results for the side-on species first and then for the end-on complexes.

Side-On Quintet Complexes. $^5\mathbf{I}_{side\text{-}on}$ is related to $^7\mathbf{I}_{side\text{-}on}$, since they share a similar electronic configuration as shown in Table 1 and Figure 4; $^7\mathbf{I}_{side\text{-}on}$ has an F coupling of the superoxo electron (in the O_2 $\pi^*_\perp$ orbital) to the Fe(III) center (*S* = 5/2),

while $^5\mathbf{I}_{\text{side-on}}$ is the corresponding AF-coupled state. The calculated relative energy of $^5\mathbf{I}_{\text{side-on}}$ is 14.3 kcal/mol. By comparing this value with that of $^7\mathbf{I}_{\text{side-on}}$ (9.5 kcal/mol), it is clear that ferromagnetic coupling is favored over antiferromagnetic coupling for the O_2 side-on structures. The calculated vertical gap at the geometry of $^5\mathbf{I}_{\text{side-on}}$ between the higher AF-coupled quintet state and the lower F-coupled septet state is 4.2 kcal/mol.

As seen from Figure 4, $^5\mathbf{II}_{\text{side-on}}$ differs from $^5\mathbf{I}_{\text{side-on}}$ by a shift of the β singly occupied orbital from O_2 $\pi^*_\perp$ to $\pi^*_\parallel$; consequently, $\pi^*_\perp$ is doubly occupied. Formally, there are six unpaired electrons in $^5\mathbf{II}_{\text{side-on}}$. However, the overlap between $\pi^*_\parallel$ and d_{xz} (see Figure 4) is considerably better that the overlap of $\pi^*_\perp$ and any iron 3d orbital. The singlet coupling between $\pi^*_\parallel$ and the d_{xz} electron pair is therefore strong enough to lead to an Fe−O bonding (see NO occupancy in Figure 5a), albeit keeping certain radicaloid character, as revealed clearly by the corresponding spin natural orbitals (SNOs) from symmetry broken DFT calculation (see SNO in Figure 5a). Here, because of the strong bonding between the

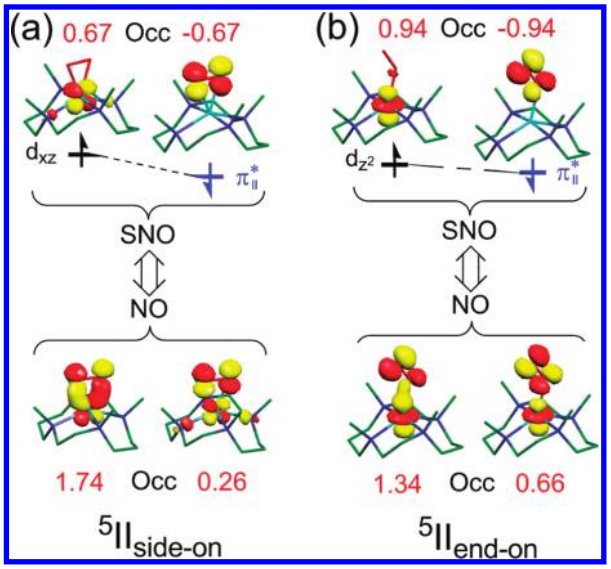

Figure 5. Spin natural orbitals (SNO) and natural orbitals (NO) describing the symmetry broken phenomenon in $^5\mathbf{II}_{\text{side-on}}$ (a) and $^5\mathbf{II}_{\text{end-on}}$ (b). Occupancy numbers are marked in red.

electrons in the $\pi^*_\parallel$ and d_{xz} orbitals, the corresponding ferromagnetically coupled septet counterpart having two α spins in the $\pi^*_\parallel$ and d_{xz}, which is devoid of Fe−O_2 bonding, should be high lying and hence could not be located. The relative energy of $^5\mathbf{II}_{\text{side-on}}$ is 21.8 kcal/mol, which is 7.5 kcal/mol higher than $^5\mathbf{I}_{\text{side-on}}$. As will be seen below from our ab initio calculations, the relative energy of $^5\mathbf{II}_{\text{side-on}}$ could be highly overestimated by B3LYP.

Another peculiarity of $^5\mathbf{II}_{\text{side-on}}$ is that its formal iron oxidation state can be assigned as Fe(IV)−peroxo. The reason for this is that unlike all other species found in this study, the $\pi^*_\perp$ orbital of the O_2 moiety in $^5\mathbf{II}_{\text{side-on}}$ is doubly occupied. As mentioned above, this observation originates from the fact that in the side-on binding mode, unlike the end-on one, $\pi^*_\perp$ can hardly have any good overlap with any iron d orbital. Thus, among the valence shell of the O_2 moiety, the only open-shell fragment orbital (except for the fully filled ones) originates from $\pi^*_\parallel$, which mixes with d_{xz} to generate two MOs ($d_{xz} \pm \pi^*_\parallel$) containing one electron pair as seen in the two NOs in Figure 5a. It is seen that the bonding NO is populated by 1.74e, which is approximately a double occupancy, while the antibonding NO has a small population. This picture is consistent with the small SNO population, and the case can be contrasted with the end-on complex in Figure 5b. The Fe−O bond lengths in $^5\mathbf{II}_{\text{side-on}}$ are the shortest (about 2.0 Å, see Figure 2) among all the side-on structures we located in this work, which conforms to a significantly covalent Fe−O_2 bonding. The small population in the Fe−O_2 antibonding orbital shows that ferric−superoxo only has a small contribution to the electronic structure of $^5\mathbf{II}_{\text{side-on}}$. As such, the electronic structure in Figure 5a indicates that the Fe(IV)−peroxo assignment of $^5\mathbf{II}_{\text{side-on}}$ could be more appropriate than Fe(III)−superoxo.

Different from $^5\mathbf{I}_{\text{side-on}}$ and $^5\mathbf{II}_{\text{side-on}}$, $^5\mathbf{III}_{\text{side-on}}$ is a tetraradicaloid state having three singly occupied iron d orbitals (d_{xz}, d_{yz}, and d_{z^2}) and a O_2 $\pi^*_\perp$ orbital as its SOMOs. It therefore has an intermediate-spin Fe(III) center (S = 3/2) F coupled to superoxo (S = 1/2) as shown in Figure 4. The calculated energy of $^5\mathbf{III}_{\text{side-on}}$, 16.9 kcal/mol, is between those of $^5\mathbf{I}_{\text{side-on}}$ and $^5\mathbf{II}_{\text{side-on}}$. We also calculated the AF-coupled triplet counterpart (denoted in Figure 2 as $^3\mathbf{I}_{\text{side-on}}$) of $^5\mathbf{III}_{\text{side-on}}$, which has a β electron in the O_2 $\pi^*_\perp$ orbital rather than an α one as in $^5\mathbf{III}_{\text{side-on}}$. The computed vertical gap between the higher AF-coupled triplet state and the lower F-coupled quintet state at the geometry of the latter, $^5\mathbf{III}_{\text{side-on}}$, is 4.4 kcal/mol. Thus, as in the case of $^5\mathbf{I}_{\text{side-on}}$ with a vertical gap of 4.2 kcal/mol, the F coupling between the superoxo ligand and the iron center is favored over AF coupling in the O_2 side-on coordination mode. This uniform preference of F coupling over AF coupling for iron(III)−superoxo side-on species involving both an intermediate-spin (S = 3/2) ferric iron center in $^5\mathbf{III}_{\text{side-on}}$ and a high-spin (S = 5/2) ferric iron center in $^5\mathbf{I}_{\text{side-on}}$ is an interesting feature that was never reported previously. We will come back to this point later when we discuss the Fe−O_2 end-on species below.

End-On Quintet Complexes. We located three end-on states, $^5\mathbf{I}_{\text{end-on}}$, $^5\mathbf{II}_{\text{end-on}}$, and $^5\mathbf{III}_{\text{end-on}}$, having electronic structures virtually the same as the corresponding side-on ones (see Figure 4 for side-on ones). The only qualitative difference was found for $^5\mathbf{II}_{\text{end-on}}$ vs $^5\mathbf{II}_{\text{side-on}}$; the former involves singlet coupling of the $\pi^*_\parallel$:d_{z^2} orbital pair, whereas the latter involves singlet coupling of the $\pi^*_\parallel$:d_{xz} orbital pair. This difference originates from the different optimal orbital overlap between iron and O_2 moieties in side-on and end-on coordination modes, as shown schematically in Scheme 2.

Scheme 2. Optimal Orbital Overlaps between O_2 $\pi^*_\parallel$ and Iron d Orbitals in Side-On and End-On Modes

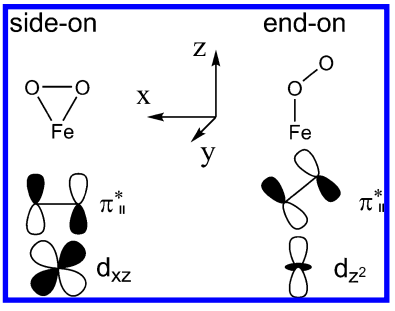

One consequence of this difference is that symmetry breakage is more severe in $^5\mathbf{II}_{\text{end-on}}$ than in $^5\mathbf{II}_{\text{side-on}}$, as shown in the SNO occupancy in Figure 5, which reveals that the coupling between

dx.doi.org/10.1021/ct300015y | J. Chem. Theory Comput. 2012, 8, 915−926

$\pi^*_{\|}$ and d_{z^2} in $^5\mathbf{II}_{\text{end-on}}$ is weaker than the coupling between $\pi^*_{\|}$ and d_{xz} in $^5\mathbf{II}_{\text{side-on}}$, possibly due to different orbital levels of iron d_{z^2} and d_{xz}. The weak coupling between $\pi^*_{\|}$:d_{z^2} is also confirmed by the small vertical gap of just 1.0 kcal/mol between AF-coupled $^5\mathbf{II}_{\text{end-on}}$ and the corresponding F-coupled septet state lying above $^5\mathbf{II}_{\text{end-on}}$. Comparatively, the corresponding F-coupled septet state of $^5\mathbf{II}_{\text{side-on}}$ could not be located, possibly because of its high energy above $^5\mathbf{II}_{\text{side-on}}$ due to the strong bonding of the $\pi^*_{\|}$ and d_{xz} orbital pair. The calculated relative energies show that $^5\mathbf{I}_{\text{end-on}}$/$^5\mathbf{III}_{\text{end-on}}$ are slightly lower/higher in energy than $^5\mathbf{I}_{\text{side-on}}$/$^5\mathbf{III}_{\text{side-on}}$, respectively, while $^5\mathbf{II}_{\text{end-on}}$ is significantly lower than $^5\mathbf{II}_{\text{side-on}}$ by ∼8 kcal/mol.

As we demonstrated above for the side-on species, F coupling between $\pi^*_{\perp}$ of O_2^- and the Fe(III) center is favored in energy over AF coupling. Then, what is the situation in the end-on species? For the medium-spin (S = 3/2) ferric center $^5\mathbf{III}_{\text{end-on}}$ the corresponding AF-coupled triplet state is vertically 2.4 kcal/mol higher; for the high-spin (S = 5/2) ferric center $^5\mathbf{I}_{\text{end-on}}$ the corresponding F-coupled septet state is vertically 0.9 kcal/mol lower. Thus, at first glance, it appears that AF coupling is also disfavored in end-on cases as in the side-on cases. However, upon checking the geometries of $^5\mathbf{III}_{\text{end-on}}$ and $^5\mathbf{I}_{\text{end-on}}$ in Figure 2 we found that the Fe−O−O angle, which represents the degree of "bending down" of FeO_2 from end-on toward the side-on mode, is apparently smaller than 145°. The ∠Fe−O−O is about 113°/119° in $^5\mathbf{III}_{\text{end-on}}$/$^5\mathbf{I}_{\text{end-on}}$. To test if this Fe−O−O angle really determines the preference of the coupling mode, we calculated the septet−quintet gap of $^5\mathbf{I}_{\text{end-on}}$ at the geometry optimized in the gas phase, which has a larger ∠Fe−O−O of 143°. The resulting gap between the AF-coupled quintet state and the F-coupled septet state is 0.7 kcal/mol, with the AF state being lower than the F state. Thus, as demonstrated in Figure 6, it is clear that the preference of either

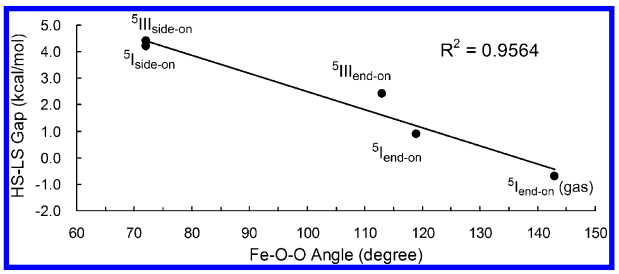

Figure 6. Dependence of the HS−LS gap between the pair of iron(III)−superoxo F-/AF-coupled states on ∠Fe−O−O in $[(TMC)Fe(O_2)]^{2+}$. Positive gap means a lower HS (F-coupled) state, and a negative one means a lower LS (AF-coupled) state.

the F or the AF state is dependent on the ∠Fe−O−O angle, i.e., the degree of Fe−O_2 "bending-down". The ∠Fe−O−O angles of $^5\mathbf{III}_{\text{side-on}}$, $^5\mathbf{I}_{\text{side-on}}$, $^5\mathbf{III}_{\text{end-on}}$, $^5\mathbf{I}_{\text{end-on}}$, and the gas-phase-optimized $^5\mathbf{I}_{\text{end-on}}$ are about 72°, 72°, 113°, 119°, 143°, respectively; correspondingly, the gaps from AF- to F-coupled states are 4.4, 4.2, 2.4, 0.9, and −0.7 kcal/mol, respectively. Thus, the more side-on character the species has, the greater its preference for F coupling is within the examined angle range. The contrary is also true; the more end-on character the species has, the greater its preference for AF coupling is. This finding underscores the recent experimental identification of the AF state for ferric−superoxo species in non-heme enzyme 2,3-HPCD, which was assigned to the end-on iron(III)−superoxo species.[8] This FeOO angle dependence of the exchange coupling between the superoxo radical and Fe(III) may well be the origin of both the previous computational findings of the sensitivity of exchange coupling to the protein environment and the inconsistency of the previous DFT calculation with experiment about the sign of the exchange coupling constant.[8]

Triplet States (S = 1). *Side-on Triplet Complex.* The corresponding AF-coupled state of $^5\mathbf{III}_{\text{side-on}}$, denoted as $^3\mathbf{I}_{\text{side-on}}$ (in Figure 2), was located, and its electronic configuration is shown in Figure 7. The calculated relative energy is 21.8 kcal/mol. Although we explored other side-on triplet electronic configurations, no other minimum could be located in geometry optimizations.

End-On Triplet Complexes. Among the two energetically lowest end-on triplet state species, $^3\mathbf{I}_{\text{end-on}}$ has the same configuration as $^3\mathbf{I}_{\text{side-on}}$, i.e., the one corresponding to the AF state of $^5\mathbf{III}_{\text{end-on}}$. $^3\mathbf{I}_{\text{end-on}}$ is 2.5 kcal/mol lower than $^3\mathbf{I}_{\text{side-on}}$ in energy. The second end-on triplet state, $^3\mathbf{II}_{\text{end-on}}$, is different from $^3\mathbf{I}_{\text{end-on}}$ by change of the singly occupied β orbital from $\pi^*_{\perp}$ to $\pi^*_{\|}$, which consequently makes $\pi^*_{\perp}$ doubly occupied. Their connection is similar to the ones noted between $^5\mathbf{I}_{\text{end-on}}$ and $^5\mathbf{II}_{\text{end-on}}$ and between $^5\mathbf{I}_{\text{side-on}}$ and $^5\mathbf{II}_{\text{side-on}}$, as shown in Figure 7. $^3\mathbf{II}_{\text{end-on}}$ is 1.8 kcal/mol higher in energy than $^3\mathbf{I}_{\text{end-on}}$.

Singlet States (S = 0). For the singlet state, we obtained only one tetraradicaloid species, $^1\mathbf{I}_{\text{end-on}}$, with an intermediate-spin Fe(II) (S = 1) AF coupled with the triplet O_2, as shown in Figure 5. This is the only O_2-bound Fe(II)(O_2) species that we obtained, and its relative energy is 17.3 kcal/mol.

CCSD(T) Calibration. To estimate the accuracy of our DFT (B3LYP/B2) approach, we carried out extensive RCCSD(T) calculations on the truncated model system $[(NH_3)_4Fe(O_2)]^{2+}$ of $[(TMC)Fe(O_2)]^{2+}$. This comparison between the DFT results, obtained at a frequently adopted level in transition-metal systems, and RCCSD(T) results is meaningful. The results of our RCCSD(T) computations, with CBS limit extrapolation and iron 3s3p correlation correction, are summarized in Table 2, alongside the B3LYP/B2 results for exactly the same model and geometries. For those AF-coupled states, like $^5\mathbf{I}_{\text{side-on}}$, $^5\mathbf{I}_{\text{end-on}}$, $^5\mathbf{II}_{\text{end-on}}$, $^3\mathbf{I}_{\text{side-on}}$, $^3\mathbf{I}_{\text{end-on}}$, $^3\mathbf{II}_{\text{end-on}}$, and $^1\mathbf{I}_{\text{end-on}}$, wherein severe symmetry breakage occurs in DFT, RCCSD(T) cannot have an appropriate reference configuration. Thus, we cannot calculate these states with RCCSD(T). For almost all those states except $^1\mathbf{I}_{\text{end-on}}$ we could locate a F-coupled high-spin state that has the same configuration as the AF-coupled states. Among them, the corresponding F-coupled states of $^5\mathbf{I}_{\text{side-on}}$, $^3\mathbf{I}_{\text{side-on}}$, and $^3\mathbf{I}_{\text{end-on}}$ are just $^7\mathbf{I}_{\text{side-on}}$, $^5\mathbf{III}_{\text{side-on}}$, and $^5\mathbf{III}_{\text{end-on}}$, respectively. Thus, assuming that the geometry difference contribution to the energy errors is minor, we can just use the CCSD(T) energy corrections of the latter three states to estimate the accuracy of B3LYP for the former three states, which share the same configurations with the latter three. For the other three states, i.e., $^5\mathbf{I}_{\text{end-on}}$, $^5\mathbf{II}_{\text{end-on}}$, and $^3\mathbf{II}_{\text{end-on}}$, we calculate their F-coupled counterpart to assess the performance of B3LYP for these types of configurations.

To aid the following discussion we show in Figure 8 the relative energies of the common species using the B3LYP and CCSD(T) results of Tables 1 and 2. Thus, from Figure 8 and the results in Table 2 we can deduce that the B3LYP/B2 results are reasonably close to CCSD(T)/CBS results for most states, like $^7\mathbf{I}_{\text{side-on}}$, $^5\mathbf{III}_{\text{side-on}}$, $^5\mathbf{I}_{\text{end-on}}$, $^5\mathbf{II}_{\text{end-on}}$, and $^3\mathbf{II}_{\text{end-on}}$ (see small $\Delta\Delta E$ values for these states). From previous discussions this also implies that the relative B3LYP/B2 energies of $^5\mathbf{I}_{\text{side-on}}$ (having the same configuration as $^7\mathbf{I}_{\text{side-on}}$) and $^3\mathbf{I}_{\text{side-on}}$ (having the same configuration as $^5\mathbf{III}_{\text{side-on}}$) are less likely to have

dx.doi.org/10.1021/ct300015y | J. Chem. Theory Comput. 2012, 8, 915−926

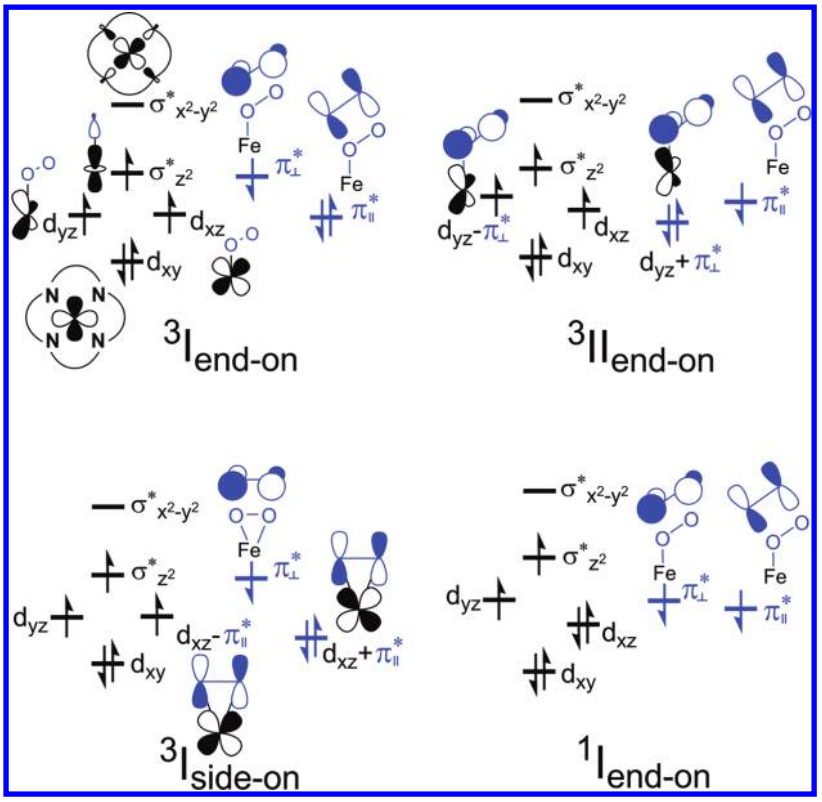

Figure 7. Electronic configurations of triplet and singlet states of $[(TMC)Fe(O_2)]^{2+}$.

Table 2. Calculated Relative Energies of the $[(NH_3)_4Fe(O_2)]^{2+}$ Model Truncated from $[(TMC)Fe(O_2)]^{2+}$ at the RCCSD(T)/CBS and B3LYP/B2 Levels in the Gas Phase, CCSD(T) Corrections ($\Delta\Delta E$) for B3LYP/B2, and B3LYP/CPCM/B2 Energies of $[(TMC)Fe(O_2)]^{2+}$ with CCSD(T) Corrections

	$^7\mathbf{I}_{unbound}$	$^7\mathbf{I}_{side\text{-}on}$	$^5\mathbf{II}_{side\text{-}on}$	$^5\mathbf{III}_{side\text{-}on}$	$^5\mathbf{I}_{end\text{-}on}$ [c]	$^5\mathbf{II}_{end\text{-}on}$ [c]	$^5\mathbf{III}_{end\text{-}on}$	$^3\mathbf{II}_{end\text{-}on}$ [d]
RCCSD(T)/CBS[a,b]	0.0	1.4	13.2	20.8	11.4	6.2	24.6	26.0
B3LYP/B2[b]	0.0	4.3	23.0	18.2	8.8	5.7	17.3	23.1
$\Delta\Delta E$[e]	0.0	−2.9	−9.8	2.6	2.6	0.5	7.3	2.9
B3LYP/CPCM/B2+$\Delta\Delta E$[f]	0.0	6.7	12.0	19.5	16.2	14.1	25.8	24.0

[a]The iron 3s3p correlation correction is included. [b]Truncated model $[(NH_3)_4Fe(O_2)]^{2+}$ in the gas phase. [c]The symmetry broken AF-coupled quintet states cannot be calculated with the RCCSD(T) approach; the corresponding F-coupled septet states were calculated instead. [d]The symmetry broken AF-coupled triplet states cannot be calculated with the RCCSD(T) approach; the corresponding F-coupled quintet states were calculated instead. [e]$\Delta\Delta E$ = ΔE(RCCSD(T)/CBS) − ΔE(B3LYP/B2), i.e., difference between the corresponding two levels. [f]B3LYP/CPCM/B2 values of $[(TMC)Fe(O_2)]^{2+}$ taken from Table 1 and corrected by $\Delta\Delta E$ obtained in this table.

significant errors. Among these five states, only $^7\mathbf{I}_{side\text{-}on}$ is underestimated in stability by about 3 kcal/mol with DFT, whereas all of the other four states are more or less overestimated in stability with DFT by up to about 3 kcal/mol.

Except for the above five states, which have close relative energies at the DFT and CCSD(T) levels, the energy of $^5\mathbf{III}_{end\text{-}on}$ is underestimated by B3LYP/B2 by ∼7 kcal/mol, indicating that the underestimation by such a magnitude is also likely to exist in $^3\mathbf{I}_{end\text{-}on}$ (having the same configuration as $^5\mathbf{III}_{end\text{-}on}$). On the contrary, the relative energy of $^5\mathbf{II}_{side\text{-}on}$ is overestimated by about 10 kcal/mol. This unusual large underestimation of $^5\mathbf{II}_{side\text{-}on}$ stability by B3LYP is expected by spin contamination ($\langle S^2\rangle$ = 6.46 at the B3LYP/CPCM/B2 level) of this symmetry-broken quintet state. Although the spin contamination itself is not large, it has a serious effect in energy due to the high energy of the contaminant septet state (see the above part of the DFT result for $^5\mathbf{II}_{side\text{-}on}$). With these estimates of possible errors of the B3LYP/B2 level in mind and from inspecting Table 1, the lowest bound state of (TMC)Fe−O_2 is suggested to be $^7\mathbf{I}_{side\text{-}on}$, which is ∼7 kcal/mol above the $^7\mathbf{I}_{unbound}$ reference point. The endothermicity of the (TMC)-Fe−O_2 bound state is consistent with the fact that experiment could not detect the (TMC)Fe−O_2 complex.[24−27] Moreover, a recent reactivity study on these systems confirms this endothermicity using different functionals and that the species are still relevant for the suggested reaction.[3n] Finally, we note that though B3LYP is known to underestimate Fe−O_2 binding energy in the heme system, after dispersion correction, which we also considered here, this trend does not hold any more.[40]

Below 17 kcal/mol, there are several more states, including two O_2 side-on states $^5\mathbf{I}_{side\text{-}on}$ and $^5\mathbf{II}_{side\text{-}on}$ and two O_2 end-on states $^5\mathbf{II}_{end\text{-}on}$ and $^5\mathbf{I}_{end\text{-}on}$, which (with a nominal exception of $^5\mathbf{II}_{side\text{-}on}$) are all hexaradicaloid iron(III)−superoxo quintet states having a high-spin (S = 5/2) ferric center AF-coupled with a superoxo radical in either one of the O_2^- π^* orbitals. Thus, all in all the B3LYP results provide reasonable state ordering of the manifold and the endothermicity of the bound FeO_2 complexes relative to the van der Waals $^7\mathbf{I}_{unbound}$ reference

dx.doi.org/10.1021/ct300015y | J. Chem. Theory Comput. 2012, 8, 915−926

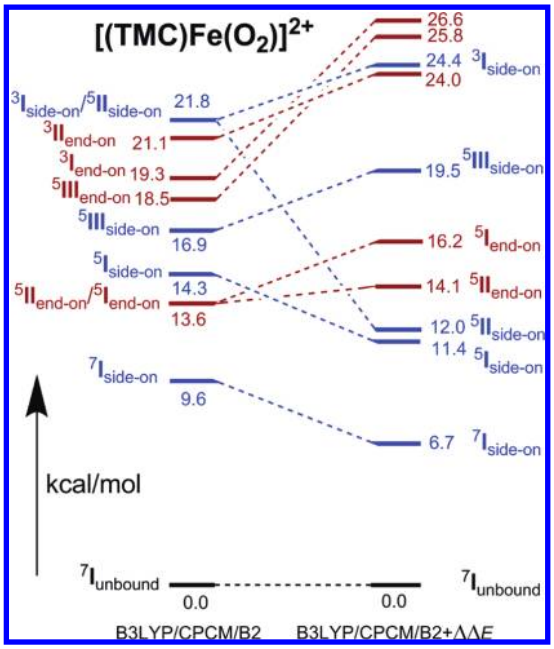

Figure 8. Diagram of relative energies of $[(TMC)Fe(O_2)]^{2+}$ for common states calculated by B3LYP/CPCM/B2 (left side) and those after embedding the corrections from the CCSD(T)/CBS level (right side).

point except in the case of ^{5}**II**$_{side\text{-}on}$. We proceed therefore to explore the B3LYP behavior of these complexes.

Solvent Effect. The above DFT results incorporate the solvation effect using the CPCM continuum solvation model and optimizing the geometry in the solvent. To explore the magnitude of the solvent effect on $[(TMC)Fe(O_2)]^{2+}$, we also performed gas-phase geometry optimizations for all Fe−O_2 states under study, which are shown in Table 3. On the basis of the recommendation to use gas-phase-optimized geometries in the continuum solvation model calculation,[41] we employed yet another continuum solvation model, SMD,[42] for comparison with the CPCM results involving geometry optimization in solvent. Comparing the gas-phase results with CPCM or SMD results in Table 3 we can see that the solvent affects significantly the O_2-binding energy. In other words, one can conclude that O_2 binding is sensitive to the solvent, while the energy differences between the O_2-bound species themselves are fairly constant. This is in line with experimental findings of the sensitivity of O_2 activation on solvents used in non-heme systems[24,25] as well as in other transition-metal systems like chromium(III) corrole.[43] Generally, the O_2-bound species are destabilized by around 10 kcal/mol or more in solvation model calculations using acetonitrile as a solvent. However, we can see that some states change their electronic configurations, like ^{5}**I**$_{end\text{-}on}$ and ^{3}**II**$_{end\text{-}on}$, when optimized in the gas phase rather than in solvent. This implies a sensitivity and flexibility of ferric−superoxo electronic states to the environment, which may lead to different behaviors in different chemical environments, e.g., non-heme enzymes and solution environments. Concerning the two adopted continuum solvation models, CPCM and SMD, the differences between them, compared to ^{7}**I**$_{unbound}$, range from 2.3 to 4.5 kcal/mol, with consistently lower relative energies by the SMD model.

Axial Ligand Binding to Ferric−Superoxo Intermediate. We investigated the 6-coordinate system $[(TMC)Fe(O_2)(MeCN)]^{2+}$, wherein a solvent molecule, acetonitrile (MeCN), is coordinated to the iron at the axial position. Table 4 summarizes our results for all states that we located in this work for this complex. It can be seen that the number of states in the 6-coordinate system reduces significantly because many tetraradicaloid states, like ^{5}**III**$_{end\text{-}on}$ and ^{5}**III**$_{side\text{-}on}$, and all triplet ones (^{3}**I**$_{side\text{-}on}$, ^{3}**I**$_{end\text{-}on}$, and ^{3}**II**$_{end\text{-}on}$) cannot bind CH_3CN as an axial ligand. During geometry optimizations in solvent for these complexes the MeCN ligand dissociates. There are two states, ^{5}**II**$_{side\text{-}on}$ and ^{5}**I**$_{end\text{-}on}$, which both change to the ^{5}**II**$_{end\text{-}on}$ configuration after geometry optimization with MeCN added as an axial ligand. For those states which can bind MeCN as an axial ligand and keep their electronic configurations, their relative energies mostly increase by several kcal/mol, except for ^{1}**I**$_{end\text{-}on}$ which is slightly stabilized. All in all, the axial ligand MeCN has a limited effect on the relative energies of $[(TMC)Fe(O_2)]^{2+}$ if MeCN can bind and the electronic configuration is kept. For clarity and further referral, Figure 9 depicts all the states and their relative energies in the various environments for the penta- and hexacoordinated complexes. However, it should be noted that MeCN binding anti to the methyl groups is not likely since the binding energy is endothermic by 9.7 and 6.5 kcal/mol if O_2 is already bound on the other side.

Reactivity Estimations Based on the EER Principle. This is a good point where we can use all of the above data to attempt to predict the reactivity and expected behavior based on the considerations of electronic structure factors. This is done based on the exchange-enhanced reactivity (EER) principle,[44] which states that if the number of identical-spin unpaired electrons on the metal center increases in the transition state from four to five (or the orbitals get more localized on the metal center) this will maximize the exchange stabilization of the transition state. Consider now an H-abstraction process by the hexaradicaloid states ^{5}**I**/**II**$_{side\text{-}on}$ and ^{5}**I**/**II**$_{end\text{-}on}$. In these states, one of the d electrons on the Fe(III) center is coupled to the electron in the O_2 π^* orbital; hence, the net α-spin contributed by this electron to the Fe(III) center is less than one. During the H abstraction, however, an electron shifts from the σ_{CH} orbital to the O_2 π^* orbital and thereby the d electron is freed from its AF coupling and enhances the exchange on the iron center, as exemplified for ^{5}**II**$_{end\text{-}on}$ in Figure 10a. These FeO_2 states are likely to have higher intrinsic (i.e., within the

Table 3. Relative Energies (kcal/mol) of States of $[(TMC)Fe(O_2)]^{2+}$ at the B3LYP/CPCM/B2 and B3LYP/SMD/B2 Levels

model	^{7}**I**$_{unbound}$	^{7}**I**$_{side\text{-}on}$	^{5}**I**$_{side\text{-}on}$	^{5}**II**$_{side\text{-}on}$	^{5}**III**$_{side\text{-}on}$	^{5}**I**$_{end\text{-}on}$	^{5}**II**$_{end\text{-}on}$	^{5}**III**$_{end\text{-}on}$	^{3}**I**$_{side\text{-}on}$	^{3}**I**$_{end\text{-}on}$	^{3}**II**$_{end\text{-}on}$	^{1}**I**$_{end\text{-}on}$
in vacuo	0.0	−1.9	3.2	9.9	5.9	—[c]	3.1	—[d]	11.7	9.2	—[e]	1.9
CPCM[a]	0.0	9.6	14.3	21.8	16.9	13.6	13.6	18.5	21.8	19.3	21.1	17.3
SMD[b]	0.0	6.0	10.4	18.3	13.0	—[c]	10.9	—[d]	17.8	14.8	—[e]	15.0

[a]Optimized in solvent acetonitrile. [b]Geometries optimized in the gas phase; for comparison with CPCM, minor nonelectrostatic contributions (<0.8 kcal/mol) are not included. [c]In the gas phase, ^{5}**I**$_{end\text{-}on}$ changes to ^{5}**II**$_{end\text{-}on}$ in geometry optimization. [d]In the gas phase, O_2 dissociates in geometry optimization. [e]In the gas phase, ^{3}**II**$_{end\text{-}on}$ changes to ^{3}**I**$_{end\text{-}on}$ in geometry optimization.

Table 4. Relative Energies (kcal/mol) of States of $[(TMC)Fe(O_2)(MeCN)]^{2+}$ Compared with Corresponding $[(TMC)Fe(O_2)]^{2+}$ at the B3LYP/CPCM/B2 Level

	$^7I_{unbound}$	$^7I_{side\text{-}on}$	$^5I_{side\text{-}on}$	$^5II_{side\text{-}on}$	$^5III_{side\text{-}on}$	$^5I_{end\text{-}on}$	$^5II_{end\text{-}on}$	$^5III_{end\text{-}on}$	$^3I_{side\text{-}on}$	$^3I_{end\text{-}on}$	$^3II_{end\text{-}on}$	$^1I_{end\text{-}on}$
$[(TMC)Fe(O_2)]^{2+}$	0.0	9.6	14.3	21.8	16.9	13.6	13.6	18.5	21.8	19.3	21.1	17.3
$[(TMC)Fe(O_2)(MeCN)]^{2+}$	0.0	12.3	18.3	—[a]	—[b]	—[a]	17.3	—[b]	—[b]	—[b]	—[b]	16.8

[a]Change to $^5II_{end\text{-}on}$ configuration in geometry optimization. [b]MeCN dissociates in geometry optimization.

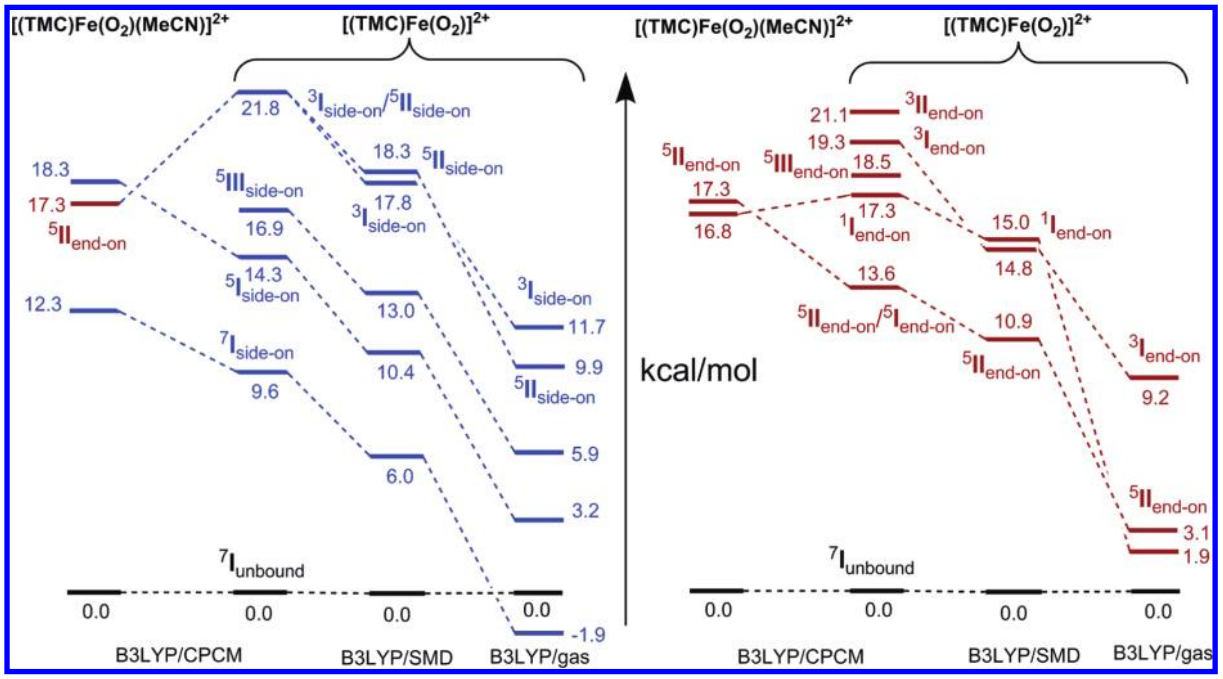

Figure 9. B3LYP/B2 relative energies of various species calculated in acetonitrile with the CPCM and SMD solvation model and in the gas phase: (left, blue) side-on complexes and (right, brown) end-on species. For all complexes, we show the state ordering for the pentacoordinated $[(TMC)Fe(O_2)]^{2+}$ and the hexacoordinate $[(TMC)Fe(O_2)(MeCN)]^{2+}$, where the sixth ligand is an acetonitrile molecule.

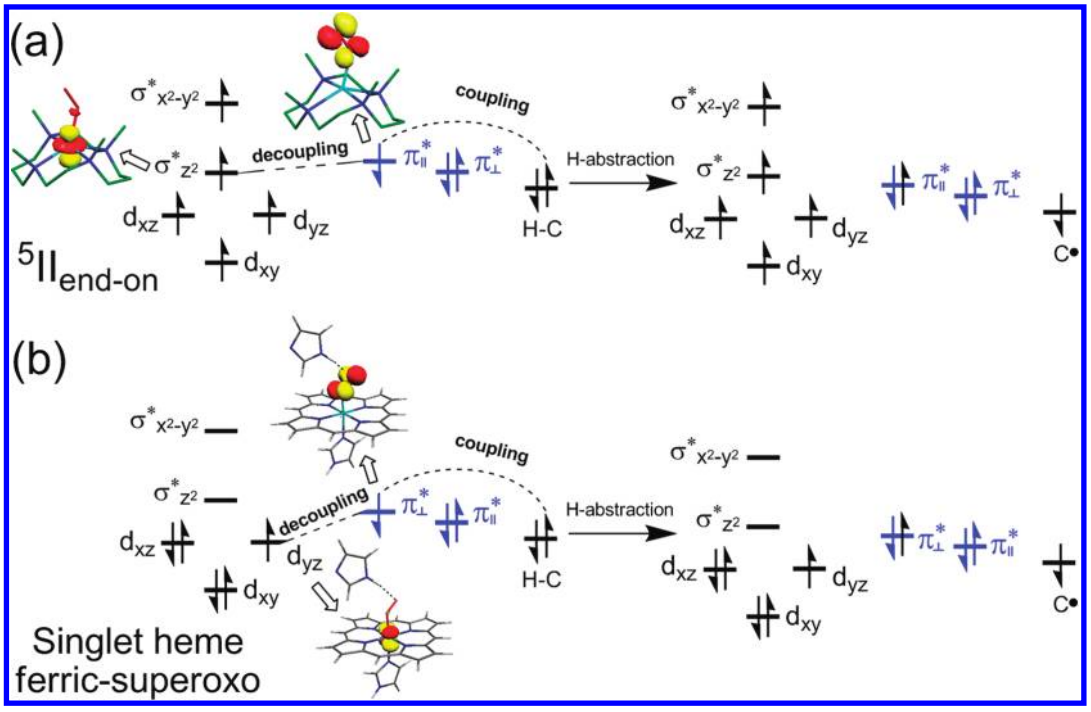

Figure 10. (a) EER of H abstraction from $[(TMC)Fe(O_2)]^{2+}$ exemplified with $^5II_{end\text{-}on}$, and (b) comparison with the heme ferric−superoxo system.

same spin state) H-abstraction reactivity relative to others. By contrast, in heme−O_2 complexes as shown in Figure 10b, where the ground state is singlet, the reactivity is sluggish compared to the high-valent iron−oxo species,[9d,13d] which can

dx.doi.org/10.1021/ct300015y | J. Chem. Theory Comput. 2012, 8, 915−926

be understood by lacking the EER opportunity due to the electronic structure. We note that the products of the H abstraction by $[(TMC)Fe(O_2)]^{2+}$ and heme systems, i.e., ferric−hydroperoxo (Fe(III)OOH) species, were experimentally determined as HS (S = 5/2)[4i] and LS (S = 1/2)[45,46] states, respectively, which is fully consistent with the current reactivity scenario in Figure 10. The suggestion that the high-spin (S = 5/2) iron center of all these electronic structures has a high reactivity due to EER is in line with the experimental identification of the crucial role of the high-spin non-heme Fe(II) center in O_2 activation.[24,25] The iron(III)−superoxo character of these $[(TMC)Fe(O_2)]^{2+}$ species also highlights the previous finding about the importance of the redox potential of non-heme Fe(II) reagent in O_2 activation because one straightforward electron transfer from Fe(II) to O_2 is involved to generate the ferric−superoxo species.[24,25]

IV. CONCLUSIONS

This study focuses on an experimentally intriguing non-heme ferric−superoxo system $[(TMC)Fe(O_2)]^{2+}$, which was proposed before by one of us to perform allylic C−H activation.[26] The explored spin states of this species cover the whole range from S = 0 to S = 3, within about 25 kcal/mol, with complexes having Fe−O_2 with side-on- and end-on-coordinated O_2. Unlike the well-studied non-heme ferryl−oxo species, which mainly concern two low-lying spin states of S = 2 and 1, and unlike the heme−superoxo which usually has a singlet ground state, the $[(TMC)Fe(O_2)]^{2+}$ species is found here to have much richer and complex electronic structure with at least 12 different species that we could locate.

This rich electronic structure can form the basis of a broad picture for non-heme ferric−superoxo complexes. For example, a recent theoretical work by Morokuma et al. explored the reactivity of three states of $[(TMC)Fe(O_2)]^{2+}$, i.e., $^7\mathbf{I}_{side\text{-}on}$, $^5\mathbf{I}_{side\text{-}on}$, and $^5\mathbf{II}_{end\text{-}on}$,[13d] which are all included among the states we located here. Most previous theoretical studies[13−15] of ferric−superoxo complexes mainly focused on the electronic structure of the high-spin (S = 5/2) Fe(III) center coupled to superoxo, which are fully covered by this study. The various chemical environments in various non-heme ferric−superoxo species may lead in turn to various state-specific stabilization for those states we obtained in this work, and as a result ferric−superoxo species can exhibit rich chemical and spectroscopic characters, which awaits further studies for specific cases. Despite the generalized picture of ferric−superoxo electronic structures portrayed in this work, it should be noted that unusual iron ligating atoms other than N and O, like the S of cysteine in non-heme enzyme cysteine dioxygenase,[16] could significantly affect the electronic structures of ferric−superoxo species and lead to heme-like ones,[6d,e] possibly due to the strong ligand field caused by the S atom.

The CCSD(T) results of a model complex are used to calibrate the DFT results. Thus, the lowest Fe−O_2 binding state of $[(TMC)Fe(O_2)]^{2+}$ is determined to be the septet (S = 3) O_2 side-on complex $^7\mathbf{I}_{side\text{-}on}$. Above this lowest state by just about 5−7 kcal/mol there are four closely lying side-on and end-on quintet (S = 2) $[(TMC)Fe(O_2)]^{2+}$ states. Except for one quintet side-on state and a singlet end-on state, all of the other 10 states are iron(III)−superoxo states. Surprisingly, the quintet side-on state $^5\mathbf{II}_{side\text{-}on}$ in this study is formally a Fe(IV)−peroxo state, which has never been reported before. The relative energy of $^5\mathbf{II}_{side\text{-}on}$ compared to $^7\mathbf{I}_{side\text{-}on}$ at the CCSD(T)-corrected DFT level is only about 5 kcal/mol, and this state is proposed here to potentially contribute to the H-abstraction reactivity of $[(TMC)Fe(O_2)]^{2+}$ by a proton-coupled electron-transfer (PCET) process. In future experimental and theoretical studies, this possibility deserves further exploration.

Another novel finding of this work is that the degree of preference of the coupling mode between the superoxo radical and the ferric iron center depends on the degree of "bending" of the O_2 moiety. We believe that this trend is general in iron(III)-superoxo systems. Whether or not this trend holds true in other transition metal−superoxo systems is an intriguing issue to be clarified in future study. Tilt in the side-on direction will favor ferromagnetic coupling, while the opposite is true for change toward the end-on structure. The effect of the sixth ligand is investigated using $[(TMC)(CH_3CN)Fe(O_2)]^{2+}$, and it is found that many of the states are not present since some of them cannot coordinate the sixth ligand. Other than that, the energetic effect of the sixth ligand is small for the states that keep their electronic configurations.

Previous experimental findings of the key roles of solvent effect, spin state, and redox potential of non-heme Fe(II) complex in O_2 activation are all corroborated in this work. The solvent effect is found to have a great impact on O_2 binding to $[(TMC)Fe(II)]^{2+}$, as compared with the gas phase; O_2-bound $[(TMC)Fe(O_2)]^{2+}$ species in acetonitrile solvent are all destabilized relative to the O_2-unbound one. The calculated endothermicity of all O_2-bound states relative to O_2-unbound one is also in line with the inability to experimentally detect an O_2-bound $[(TMC)Fe(O_2)]^{2+}$. The high-spin (S = 2) of Fe(II) center is important because for the low-lying ferric−superoxo states found in this study almost all have a high-spin (S = 5/2) ferric center, which can be straightforwardly generated from 1-electron oxidation of high-spin Fe(II) without involving spin inversion.

Finally, based on the recently proposed exchange-enhanced reactivity (EER)[44] principle, the potentially high H-abstraction reactivity of some species is suggested, which is contrasted to the heme−superoxo reactivity where the ground state is a singlet state. In fact, heme−superoxo complexes, which have singlet ground states, are generally expected to exhibit low intrinsic reactivity. The detailed results presented in this study of non-heme ferric−superoxo species may lead to a better understanding of its reactivity patterns in future experimental and theoretical studies.

■ ASSOCIATED CONTENT

Supporting Information

Cartesian coordinates, Tables S1 and S2 for energies and spin population of the various species. This material is available free of charge via the Internet at http://pubs.acs.org.

■ AUTHOR INFORMATION

Corresponding Author

*E-mail: chenh@iccas.ac.cn (H.C.); wwnam@ewha.ac.kr (W.N.); sason@yfaat.ch.huji.ac.il (S.S.).

Notes

The authors declare no competing financial interest.

■ ACKNOWLEDGMENTS

H.C. is supported by the Chinese Academy of Sciences, S.S. is supported by the Israel Science Foundation Grant 53/09, and W.N. thanks the NRF/MEST of Korea through CRI, GRL (2010-00353), and WCU (R31-2008-000-10010-0).

REFERENCES

(1) For non-heme iron enzymes, see: (a) Costas, M.; Mehn, M. P.; Jensen, M. P.; Que, L. Jr. *Chem. Rev.* **2004**, *104*, 939−986. (b) Kovaleva, E. G.; Neibergall, M. B.; Chakrabarty, S.; Lipscomb, J. D. *Acc. Chem. Res.* **2007**, *40*, 475−483. (c) Krebs, C.; Fujimori, D. G.; Walsh, C. T.; Bollinger, J. M. Jr. *Acc. Chem. Res.* **2007**, *40*, 484−492. (d) Bruijnincx, P. C. A.; van Koten, G.; Gebbink, R. J. M. K. *Chem. Soc. Rev.* **2008**, *37*, 2716−2744. (e) Ryle, M. J.; Hausinger, R. P. *Curr. Opin. Chem. Biol.* **2002**, *6*, 193−201. (f) Abu-Omar, M. M.; Loaiza, A.; Hontzeas, N. *Chem. Rev.* **2005**, *105*, 2227−2252. (g) Solomon, E. I.; Brunold, T. C.; Davis, M. I.; Kemsley, J. N.; Lee, S.-K.; Lehnert, N.; Neese, F.; Skulan, A. J.; Yang, Y.-S.; Zhou, J. *Chem. Rev.* **2000**, *100*, 235−349. (h) Solomon, E. I.; Wong, S. D.; Liu, L. V.; Decker, A.; Chow, M. S. *Curr. Opin. Chem. Biol.* **2009**, *13*, 99−113. (i) Koehntop, K. D.; Emerson, J. P.; Que, L. Jr. *J. Biol. Inorg. Chem.* **2005**, *10*, 87−93. (j) Kovaleva, E. G.; Lipscomb, J. D. *Nat. Chem. Biol.* **2008**, *4*, 186−193.

(2) For non-heme high-valent Fe(IV)(O), (a) Nam, W. *Acc. Chem. Res.* **2007**, *40*, 522−531. (b) Que, L. Jr. *Acc. Chem. Res.* **2007**, *40*, 493−500. (c) Shan, X.; Que, L. Jr. *J. Inorg. Biochem.* **2006**, *100*, 421−433. (d) Que, L. Jr.; Tolman, W. B. *Nature* **2008**, *455*, 333−340. (e) Kryatov, S. V.; Rybak-Akimova, E. V.; Schinder, S. *Chem. Rev.* **2005**, *105*, 2175−2226. (f) Rohde, J.-U.; In, J.-H.; Lim, M. H.; Brennessel, W. W.; Bukowski, M. R.; Stubna, A.; Münck, E.; Nam, W.; Que, L. Jr. *Science* **2003**, *299*, 1037−1039. (g) Bukowski, M. R.; Koehntop, K. D.; Stubna, A.; Bominaar, E. L.; Halfen, J. A.; Münck, E.; Nam, W.; Que, L. Jr. *Science* **2005**, *310*, 1000−1002. (k) Joseph, C. A.; Maroney, M. J. *Chem. Commun.* **2007**, 3338−3349.

(3) For theoretical studies on non-heme high-valent Fe(IV)(O), see: (a) Shaik, S.; Hirao, H.; Kumar, D. *Acc. Chem. Res.* **2007**, *40*, 532−542 and references therein. (b) Bassan, A.; Blomberg, M. R. A.; Borowski, T.; Siegbahn, P. E. M. *J. Inorg. Biochem.* **2006**, *100*, 727−743. (c) Schöneboom, J. C.; Neese, F.; Thiel, W. *J. Am. Chem. Soc.* **2005**, *127*, 5840−5853. (d) Decker, A.; Clay, M. D.; Solomon, E. I. *J. Inorg. Biochem.* **2006**, *100*, 697−706. (e) Decker, A.; Rohde, J.-U.; Klinker, E. J.; Wong, S. D.; Que, L. Jr.; Solomon, E. I. *J. Am. Chem. Soc.* **2007**, *129*, 15983−15996. (f) Ye, S.; Neese, F. *Curr. Opin. Chem. Biol.* **2009**, *13*, 89−98. (g) Ye, S. F.; Neese, F. *Proc. Natl. Acad. Sci. U.S.A.* **2011**, *108*, 1228−1233. (h) Banse, F.; Girerd, J.-J.; Robert, V. *Eur. J. Inorg. Chem.* **2008**, 4786−4791. (i) Ensing, B.; Buda, F.; Gribnau, M. C. M.; Baerends, E. J. *J. Am. Chem. Soc.* **2004**, *126*, 4355−4365. (j) Janardanan, D.; Usharani, D.; Chen, H.; Shaik, S. *J. Phys. Chem. Lett.* **2011**, *2*, 2610−2617. (k) Janardanan, D.; Wang, Y.; Schyman, P.; Que, L. Jr.; Shaik, S. *Angew. Chem., Int. Ed.* **2010**, *49*, 3342−3345. (l) Cho, K.-B.; Shaik, S.; Nam, W. *Chem. Commun.* **2010**, *46*, 4511−4513. (m) Usharani, D.; Janardanan, D.; Shaik, S. *J. Am. Chem. Soc.* **2011**, *133*, 176−179. (n) Cho, K.-B.; Chen, H.; Janardanan, D.; de Visser, S. P.; Shaik, S.; Nam, W. *Chem. Commun.* **2012**, *48*, 2189−2191. (o) Michel, C.; Baerends, E. J. *Inorg. Chem.* **2009**, *48*, 3628−3638.

(4) For non-heme high-valent Fe(V)(O), see: (a) de Oliveira, F. T.; Chanda, A.; Banerjee, D.; Shan, X.; Mondal, S.; Que, L. Jr.; Bominaar, E. L.; Münck, E.; Collins, T. J. *Science* **2007**, *315*, 835−838. (b) Kundu, S.; Van Kirk Thompson, J.; Ryabov, A. D.; Collins, T. J. *J. Am. Chem. Soc.* **2011**, *133*, 18546−18549. (c) Das, P.; Que, L. Jr. *Inorg. Chem.* **2010**, *49*, 9479−9485 and references therein. (d) Costas, M.; Chen, K.; Que, L. Jr. *Coord. Chem. Rev.* **2000**, *200*, 517−544. (e) Yoon, J.; Wilson, S. A.; Jang, Y. K.; Seo, M. S.; Nehru, K.; Hedman, B.; Hodgson, K. O.; Bill, E.; Solomon, E. I.; Nam, W. *Angew. Chem., Int. Ed.* **2009**, *48*, 1257−1260. (f) Makhlynets, O. V.; Rybak-Akimova, E. V. *Chem.—Eur. J.* **2010**, *16*, 13995−14006. (g) Lee, S. H.; Han, J. H.; Kwak, H.; Lee, S. J.; Lee, E. Y.; Kim, H. J.; Lee, J. H.; Bae, C.; Lee, S. N.; Kim, Y.; Kim, C. *Chem.—Eur. J.* **2007**, *13*, 9393−9398. (h) Chow, T. W.-S.; Wong, E. L.-M.; Guo, Z.; Liu, Y.; Huang, J.-S.; Che, C.-M. *J. Am. Chem. Soc.* **2010**, *132*, 13229−13239. (i) Li, F.; Meier, K. K.; Cranswick, M. A.; Chakrabarti, M.; Van Heuvelen, K. M.; Münck, E.; Que, L. Jr. *J. Am. Chem. Soc.* **2011**, *133*, 7256−7259. (j) Mas-Ballesté, R.; Que, L. Jr. *J. Am. Chem. Soc.* **2007**, *129*, 15964−15972. (k) Lyakin, O. Y.; Bryliakov, K. P.; Britovsek, G. J.; Talsi, E. P. *J. Am. Chem. Soc.* **2009**, *131*, 10798−10799. (l) Lyakin, O. Y.; Bryliakov, K. P.; Talsi, E. P. *Inorg. Chem.* **2011**, *50*, 5526−5538. (m) Prat, I.; Mathieson, J. S.; Güell, M.; Ribas, X.; Luis, J. M.; Cronin, L.; Costas, M. *Nat. Chem.* **2011**, *3*, 788−793.

(5) For theoretical studies on non-heme high-valent Fe(V)(O), see: (a) Bassan, A.; Blomberg, M. R. A.; Siegbahn, P. E. M.; Que, L. Jr. *Chem.—Eur. J.* **2005**, *11*, 692−705. (b) Bassan, A.; Blomberg, M. R. A.; Siegbahn, P. E. M.; Que, L. Jr. *J. Am. Chem. Soc.* **2002**, *124*, 11056−11063. (c) Bassan, A.; Blomberg, M. R. A.; Siegbahn, P. E. M.; Que, L. Jr. *Angew. Chem., Int. Ed.* **2005**, *44*, 2939−2941. (d) Quiñonero, D.; Morokuma, K.; Musaev, D. G.; Mas-Ballesté, R.; Que, L. Jr. *J. Am. Chem. Soc.* **2005**, *127*, 6548−6549. (e) Ma, Y.; Balbuena, P. B. *J. Phys. Chem. B* **2007**, *111*, 2711−2718. (f) de Visser, S. P.; Nam, W. *J. Phys. Chem. A* **2008**, *112*, 12887−12895. (g) Berry, J. F.; DeBeer George, S.; Neese, F. *Phys. Chem. Chem. Phys.* **2008**, *10*, 4361−4374.

(6) (a) Pauling, L.; Coryell, C. D. *Proc. Natl. Acad. Sci. U.S.A.* **1936**, *22*, 210−216. (b) Collman, J. P.; Gagne, R. R.; Reed, C. A.; Robinson, W. T.; Rodley, G. A. *Proc. Natl. Acad. Sci. U.S.A.* **1974**, *71*, 1326−1329. (c) Collman, J. P.; Gagne, R. R.; Reed, C. A.; Halbert, T. R.; Lang, G.; Robinson, W. T. *J. Am. Chem. Soc.* **1975**, *97*, 1427−1439. (d) Unno, M.; Chen, H.; Kusama, S.; Shaik, S.; Ikeda-Saito, M. *J. Am. Chem. Soc.* **2007**, *129*, 13394−13395. (e) Chen, H.; Ikeda-Saito, M.; Shaik, S. *J. Am. Chem. Soc.* **2008**, *130*, 14778−14790.

(7) Karlsson, A.; Parales, J. V.; Parales, R. E.; Gibson, D. T.; Eklund, H.; Ramaswamy, S. *Science* **2003**, *299*, 1039−1042.

(8) Mbughuni, M. M.; Chakrabarti, M.; Hayden, J. A.; Bominaar, E. L.; Hendrich, M. P.; Münck, E.; Lipscomb, J. D. *Proc. Natl. Acad. Sci. U.S.A.* **2010**, *107*, 16788−16793.

(9) (a) Chung, L. W.; Li, X.; Sugimoto, H.; Shiro, Y.; Morokuma, K. *J. Am. Chem. Soc.* **2008**, *130*, 12299−12309. (b) Chung, L. W.; Li, X.; Sugimoto, H.; Shiro, Y.; Morokuma, K. *J. Am. Chem. Soc.* **2010**, *132*, 11993−12005. (c) Lewis-Ballester, A.; Batabyal, D.; Egawa, T.; Lu, C. Y.; Lin, Y.; Marti, M. A.; Capece, L.; Estrin, D. A.; Yeh, S. R. *Proc. Natl. Acad. Sci. U.S.A.* **2009**, *106*, 17371−17376. (d) Lai, W. Z.; Shaik, S. *J. Am. Chem. Soc.* **2011**, *133*, 5444−5452. (e) Vidossich, P.; Carpena, X.; Loewen, P. C.; Fita, I.; Rovira, C. *J. Phys. Chem. Lett.* **2011**, *2*, 196−200. (f) Sen, K.; Hackett, J. C. *J. Am. Chem. Soc.* **2010**, *132*, 10293−10305. (g) Shaik, S.; Cohen, S.; Wang, Y.; Chen, H.; Kumar, D.; Thiel, W. *Chem. Rev.* **2010**, *110*, 949−1017 and references therein.

(10) (a) Kovaleva, E. G.; Lipscomb, J. D. *Science* **2007**, *316*, 453−457. (b) Mbughuni, M. M.; Chakrabarti, M.; Hayden, J. A.; Meier, K. K.; Dalluge, J. J.; Hendrich, M. P.; Münck, E.; Lipscomb, J. D. *Biochemistry* **2011**, *50*, 10262−10274.

(11) (a) Bollinger, J. M. Jr.; Krebs, C. *Curr. Opin. Chem. Biol.* **2007**, *11*, 151−158. (b) van der Donk, W. A.; Krebs, C.; Bollinger, J. M. Jr. *Curr. Opin. Struct. Biol.* **2010**, *20*, 673−683.

(12) (a) Neese, F.; Solomon, E. I. *J. Am. Chem. Soc.* **1998**, *120*, 12829−12848. (b) Brown, C. D.; Neidig, M. L.; Neibergall, M. B.; Lipscomb, J. D.; Solomon, E. I. *J. Am. Chem. Soc.* **2007**, *129*, 7427−7438. (c) Schenk, G.; Pau, M. Y. M.; Solomon, E. I. *J. Am. Chem. Soc.* **2004**, *126*, 505−515. (d) Sun, N.; Liu, L. V.; Dey, A.; Villar-Acevedo, G.; Kovacs, J. A.; Darensbourg, M. Y.; Hodgson, K. O.; Hedman, B.; Solomon, E. I. *Inorg. Chem.* **2011**, *50*, 427−436. (e) Pau, M. Y. M.; Davis, M. I.; Orville, A. M.; Lipscomb, J. D.; Solomon, E. I. *J. Am. Chem. Soc.* **2007**, *129*, 1944−1958. (f) Davis, M. I.; Wasinger, E. C.; Decker, A.; Pau, M. Y. M.; Vaillancourt, F. H.; Bolin, J. T.; Eltis, L. D.; Hedman, B.; Hodgson, K. O.; Solomon, E. I. *J. Am. Chem. Soc.* **2003**, *125*, 11214−11227. (g) Diebold, A. R.; Brown-Marshall, C. D.; Neidig, M. L.; Brownlee, J. M.; Moran, G. R.; Solomon, E. I. *J. Am. Chem. Soc.* **2011**, *133*, 18148−18160. (h) Diebold, A. R.; Straganz, G. D.; Solomon, E. I. *J. Am. Chem. Soc.* **2011**, *133*, 15979−15991.

(13) (a) Hirao, H.; Morokuma, K. *J. Am. Chem. Soc.* **2010**, *132*, 17901−17909. (b) Lundberg, M.; Morokuma, K. *J. Phys. Chem. B* **2007**, *111*, 9380−9389. (c) Lundberg, M.; Siegbahn, P. E. M.; Morokuma, K. *Biochemistry* **2008**, *47*, 1031−1042. (d) Chung, L. W.; Li, X.; Hirao, H.; Morokuma, K. *J. Am. Chem. Soc.* **2011**, *133*, 20076−20079. (e) Hirao, H.; Morokuma, K. *J. Am. Chem. Soc.* **2011**, *133*, 14550−14553.

(14) Nakatani, N.; Nakao, Y.; Sato, H.; Sakaki, S. *J. Phys. Chem. B* **2009**, *113*, 4826−4836.
(15) (a) Siegbahn, P. E. M.; Borowski, T. *Acc. Chem. Res.* **2006**, *39*, 729−738 and references therein. (b) Borowski, T.; Siegbahn, P. E. M. *J. Am. Chem. Soc.* **2006**, *128*, 12941−12953. (c) Bassan, A.; Borowski, T.; Schofield, C. J.; Siegbahn, P. E. M. *Chem.—Eur. J.* **2006**, *12*, 8835−8846. (d) Borowski, T.; Blomberg, M. R. A.; Siegbahn, P. E. M. *Chem.—Eur. J.* **2008**, *14*, 2264−2276.
(16) (a) de Visser, S. P. *Coord. Chem. Rev.* **2009**, *253*, 754−768 and references therein. (b) Kumar, D.; Thiel, W.; de Visser, S. P. *J. Am. Chem. Soc.* **2011**, *133*, 3869−3882.
(17) (a) Borovik, A. S. *Acc. Chem. Res.* **2007**, *40*, 475−483. (b) Shook, R. L.; Borovik, A. S. *Inorg. Chem.* **2010**, *49*, 3646−3660.
(18) Mukherjee, A.; Cranswick, M. A.; Chakrabarti, M.; Paine, T. K.; Fujisawa, K.; Münck, E.; Que, L. Jr. *Inorg. Chem.* **2010**, *49*, 3618−3628.
(19) Cho, J.; Jeon, S.; Wilson, S. A.; Liu, L. V.; Kang, E. A.; Braymer, J. J.; Lim, M. H.; Hedman, B.; Hodgson, K. O.; Valentine, J. S.; Solomon, E. I.; Nam, W. *Nature* **2011**, *478*, 502−505.
(20) (a) Cicchillo, R. M.; Zhang, H.; Blodgett, J. A. V.; Whitteck, J. T.; Li, G.; Nair, S. K.; van der Donk, W. A.; Metcalf, W. W. *Nature* **2009**, *459*, 871−875. (b) Whitteck, J. T.; Cicchillo, R. M.; van der Donk, W. A. *J. Am. Chem. Soc.* **2009**, *131*, 16225−16232.
(21) (a) Higgins, L. J.; Yan, F.; Liu, P.; Liu., H.-W.; Drennan, C. L. *Nature* **2005**, *459*, 871−875. (b) Mirica, L. M.; McCusker, K. P.; Munos, J. W.; Liu, H.-W.; Klinman, J. P. *J. Am. Chem. Soc.* **2008**, *130*, 8122−8123.
(22) Macbeth, C. E.; Golombek, A. P.; Young, V. G. Jr.; Yang, C.; Kuczera, K.; Hendrich, M. P.; Borovik, A. S. *Science* **2000**, *289*, 938−941.
(23) Macbeth, C. E.; Gupta, R.; Mitchell-Koch, K. R.; Young, V. G. Jr.; Lushington, G. H.; Thompson, W. H.; Hendrich, M. P.; Borovik, A. S. *J. Am. Chem. Soc.* **2004**, *126*, 2556−2567.
(24) Kim, S. O.; Sastri, C. V.; Seo, M. S.; Kim, J.; Nam, W. *J. Am. Chem. Soc.* **2005**, *127*, 4178−4179.
(25) Hong, S.; Lee, Y.-M.; Shin, W.; Fukuzumi, S.; Nam, W. *J. Am. Chem. Soc.* **2009**, *131*, 13910−13911.
(26) Lee, Y.-M.; Hong, S.; Morimoto, Y.; Shin, W.; Fukuzumi, S.; Nam, W. *J. Am. Chem. Soc.* **2010**, *132*, 10668−10670.
(27) Thibon, A.; England, J.; Martinho, M.; Young, V. G. Jr.; Frisch, J. R.; Guillot, R.; Girerd, J.-J.; Münck, E.; Que, L. Jr.; Banse, F. *Angew. Chem., Int. Ed.* **2008**, *47*, 7064−7067.
(28) For previous coupled cluster calculations for non-heme $Fe^{IV}O$ models, see: (a) Chen, H.; Lai, W. Z.; Shaik, S. *J. Phys. Chem. Lett.* **2010**, *1*, 1533−1540. (b) Geng, C. Y.; Ye, S. F.; Neese, F. *Angew. Chem., Int. Ed.* **2010**, *49*, 5717−5720.
(29) For previous coupled cluster calculations for non-heme $Fe^{V}O$ models, see: Chen, H.; Lai, W. Z.; Yao, J. N.; Shaik, S. *J. Chem. Theory Comput.* **2011**, *7*, 3049−3053.
(30) Frisch, M. J.; Trucks, G. W.; Schlegel, H. B.; Scuseria, G. E.; Robb, M. A.; Cheeseman, J. R.; Scalmani, G.; Barone, V.; Mennucci, B.; Petersson, G. A.; Nakatsuji, H.; Caricato, M.; Li, X.; Hratchian, H. P.; Izmaylov, A. F.; Bloini, J.; Zheng, G.; Sonnenberg, J. L.; Hada, M.; Ehara, M.; Toyota, K.; Fukuda, R.; Hasegawa, J.; Ishida, M.; Nakajima, T.; Honda, Y.; Kitao, O.; Nakai, H.; Vreven, T.; Montgomery, J. A., Jr.; Peralta, J. E.; Ogliaro, F.; Bearpark, M; Heyd, J. J.; Brothers, E.; Kudin, K. N.; Staroverov, V. N.; Kobayashi, R.; Normand, J.; Raghavachari, K.; Rendell, A.; Burant, J. C.; Iyengar, S. S; Tomasi, J.; Cossi, M.; Rega, N.; Millam, J. M.; Klene, M.; Knox, J. E.; Cross, J. B.; Bakken, V.; Adamo, C.; Jaramillo, J.; Comperts, R.; Stratmann, R. E.; Yazyev, O.; Austin, A. J.; Cammi, R.; Pomelli, C.; Ochterski, J. W.; Martin, R. L.; Morokuma, K.; Zakrzewski, V. G.; Voth, G. A.; Salvador, P.; Dannenbuerg, J. J.; Dapprich, S.; Daniels, A. D.; Farkas, O.; Foresman, J. B.; Ortiz, J. V.; Cioslowski, J.; Fox, D. J. *Gaussian 09*, revision B.01; Gaussian, Inc.: Wallingford, CT, 2009.
(31) (a) Becke, A. D. *Phys. Rev. A* **1988**, *38*, 3098−3100. (b) Lee, C.; Yang, W.; Parr, R. G. *Phys. Rev. B* **1988**, *37*, 785−789. (c) Becke, A. D. *J. Chem. Phys.* **1993**, *98*, 5648−5652. (d) Becke, A. D. *J. Chem. Phys.* **1993**, *98*, 1372−1377. (e) Stephens, P. J.; Devlin, F. J.; Frisch, M. J.; Chabalowski, C. F. *J. Phys. Chem.* **1994**, *98*, 11623−11627.
(32) (a) Barone, V.; Cossi, M. *J. Phys. Chem. A* **1998**, *102*, 1995−2001. (b) Cossi, M.; Rega, N.; Scalmani, G.; Barone, V. *J. Comput. Chem.* **2003**, *24*, 669−681.
(33) (a) Hay, J. P.; Wadt, W. R. *J. Chem. Phys.* **1985**, *82*, 299−310. (b) Friesner, R. A.; Murphy, R. B.; Beachy, M. D.; Ringlanda, M. N.; Pollard, W. T.; Dunietz, B. D.; Cao, Y. X. *J. Phys. Chem. A* **1999**, *103*, 1913−1928.
(34) Grimme, S.; Antony, J.; Ehrlich, S.; Krieg, H. *J. Chem. Phys.* **2010**, *132*, 154104.
(35) Werner, H.-J.; Knowles, P. J.; Lindh, R.; Manby, F. R.; Schütz, M.; Celani, P.; Korona, T.; Mitrushenkov, A.; Rauhut, G.; Adler, T. B.; Amos, R. D.; Bernhardsson, A.; Berning, A.; Cooper, D. L.; Deegan, M. J. O.; Dobbyn, A. J.; Eckert, F.; Goll, E.; Hampel, C.; Hetzer, G.; Hrenar, T.; Knizia, G.; Köppl, C.; Liu, Y.; Lloyd, A. W.; Mata, R. A.; May, A. J.; McNicholas, S. J.; Meyer, W.; Mura, M. E.; Nicklass, A.; Palmieri, P.; Pflüger, K.; Pitzer, R.; Reiher, M.; Schumann, U.; Stoll, H.; Stone, A. J.; Tarroni, R.; Thorsteinsson, T.; Wang, M.; Wolf, A. *MOLPRO, a package of ab initio programs*, version 2010.1; 2010; http://www.molpro.net.
(36) (a) Reiher, M.; Wolf, A. *J. Chem. Phys.* **2004**, *121*, 10945−10956. (b) Reiher, M.; Wolf, A. *J. Chem. Phys.* **2004**, *121*, 2037−2047.
(37) Helgaker, T.; Klopper, W.; Koch, H.; Noga, J. *J. Chem. Phys.* **1997**, *106*, 9639−9646.
(38) Balabanov, N. B.; Peterson, K. A. *J. Chem. Phys.* **2005**, *123*, 064107.
(39) de Jong, W. A.; Harrison, R. J.; Dixon, D. A. *J. Chem. Phys.* **2001**, *114*, 48−53.
(40) (a) Siegbahn, P. E. M.; Blomberg, M. R. A.; Chen, S.-L. *J. Chem. Theory Comput.* **2010**, *6*, 2040−2044. (b) Radoń, M.; Pierloot, K. *J. Phys. Chem. A* **2008**, *112*, 11824−11832.
(41) Ho, J.; Klamt, A.; Coote, M. L. *J. Phys. Chem. A* **2010**, *114*, 13442−13444.
(42) Marenich, A. V.; Cramer, C. J.; Truhlar, D. G. *J. Phys. Chem. B* **2009**, *113*, 6378−6396.
(43) Mahammed, A.; Gray, H. B.; Meier-Callahan, A. E.; Gross, Z. *J. Am. Chem. Soc.* **2003**, *125*, 1162−1163.
(44) Shaik, S.; Chen, H.; Janardanan, D. *Nat. Chem.* **2011**, *3*, 19−27. For the first consideration of exchange enhancement of reactivity in iron−oxo complexes, see, Hirao, H.; Kumar, D.; Thiel, W.; Shaik, S. *J. Am. Chem. Soc.* **2005**, *127*, 13007−13018.
(45) (a) Liu, J.-G.; Ohta, T.; Yamaguchi, S.; Ogura, T; Sakamoto, S.; Maeda, Y.; Naruta, Y. *Angew. Chem., Int. Ed.* **2009**, *48*, 9262−9267. (b) Liu, J.-G.; Shimizu, Y.; Ohta, T.; Naruta, Y. *J. Am. Chem. Soc.* **2010**, *132*, 3672−3673.
(46) (a) Davydov, R. M.; Makris, T. M.; Kofman, V.; Werst, D. E.; Sligar, S. G.; Hoffman, B. M. *J. Am. Chem. Soc.* **2001**, *123*, 1403−1415. (b) Davydov, R. M.; Kofman, V.; Fujii, H.; Yoshida, T.; Ikeda-Saito, M.; Hoffman, B. M. *J. Am. Chem. Soc.* **2002**, *124*, 1798−1808. (c) Ibrahim, M.; Denisov, I. G.; Makris, M.; Kincaid, J. R.; Sligar, S. G. *J. Am. Chem. Soc.* **2003**, *125*, 13714−13718.